

An artificial viscosity approach to high order entropy stable discontinuous Galerkin methods

Jesse Chan^a

^a*Department of Computational Applied Mathematics and Operations Research
Rice University, 6100 Main St, Houston, TX, 77005*

Abstract

Entropy stable discontinuous Galerkin (DG) methods improve the robustness of high order DG simulations of nonlinear conservation laws. These methods yield a semi-discrete entropy inequality, and rely on an algebraic flux differencing formulation which involves both summation-by-parts (SBP) discretization matrices and entropy conservative two-point finite volume fluxes. However, explicit expressions for such two-point finite volume fluxes may not be available for all systems, or may be computationally expensive to compute.

This paper proposes an alternative approach to constructing entropy stable DG methods using an artificial viscosity coefficient based on the local violation of a cell entropy inequality and the local entropy dissipation. The resulting method recovers the same global semi-discrete entropy inequality that is satisfied by entropy stable flux differencing DG methods. The artificial viscosity coefficients are parameter-free and locally computable over each cell, and the resulting artificial viscosity preserves both high order accuracy and a hyperbolic maximum stable time-step size under explicit time-stepping.

1. Introduction

Entropy stable discontinuous Galerkin (DG) methods significantly improve the robustness of high order DG methods for the time-dependent nonlinear conservation laws which govern high speed and compressible fluid flows [16, 28]. These methods yield a semi-discrete entropy inequality, and rely on an algebraic “flux differencing” formulation which involves summation-by-parts (SBP) operators and entropy conservative two-point finite volume fluxes [75]. However, flux differencing entropy stable DG methods face challenges related to their reliance on entropy conservative flux formulas. For example, explicit expressions for such two-point finite volume fluxes may not be available for all systems, or may be computationally expensive to compute [68, 62]. Moreover, the use of such fluxes can lead to local linear stability issues [27, 67].

In this paper, we propose a construction of entropy stable methods using artificial viscosity. This approach is motivated by observations in [53], where the authors enforced a cell entropy inequality on nodal DG methods using subcell algebraic flux correction techniques. This cell entropy inequality is identical to the cell entropy inequality satisfied by flux differencing entropy stable DG methods,

Email address: `jesse.chan@rice.edu` (Jesse Chan)

and was observed to preserve high order accuracy and deliver results which were qualitatively similar to flux differencing entropy stable schemes.

The idea of enforcing entropy stability using a vanishing viscosity is among the oldest and most popular ideas in computational fluid dynamics (CFD) [78, 57, 75, 56, 44, 7], making a comprehensive literature review difficult. However, the approach in this paper is most closely related to the well-known entropy viscosity method [35]. What distinguishes the artificial viscosity in this paper from most traditional artificial viscosity approaches is that it is intended only to restore an entropy inequality, and not to perform shock capturing (e.g., suppressing spurious oscillations in the solution due to sharp gradients or under-resolved solution features). For example, for a linear constant coefficient PDE where a standard DG formulation is already entropy/energy stable, the artificial viscosity in this paper vanishes.

The proposed artificial is also closely related to the “entropy correction” terms proposed in [1, 2] and extended in [24, 26, 58] and other papers. While these local correction terms are simpler to implement and also restore a cell entropy inequality, the artificial viscosity “corrections” proposed in this paper using consistently discretized diffusion operators appear to be more robust, especially for higher orders of approximation. Moreover, we prove that the entropy violation estimate used in this work is smaller than the estimates of entropy violation used in [2, 26, 58], resulting in less artificial viscosity being applied.

The paper proceeds as follows: Section 2 reviews nonlinear conservation laws and different forms of an entropy inequality, and Section 3 reviews a standard DG weak formulation for a nonlinear conservation law. Section 4 describes the viscous discretization and proposes an artificial viscosity coefficient which enforces a cell entropy inequality. We conclude with numerical experiments analyzing the robustness, high order accuracy, linear stability, and minimally diffusive nature of the proposed artificial viscosity in Section 6. Finally, additional numerical experiments, the derivation of a subcell version of the artificial viscosity, and comparisons with local entropy correction terms [1, 2] are included in Appendix A, Appendix B, and Appendix C.

2. Nonlinear conservation laws and entropy inequalities

The focus of this paper is on the numerical approximation of solutions to systems of nonlinear conservation laws in d dimensions

$$\frac{\partial \mathbf{u}}{\partial t} + \sum_{m=1}^d \frac{\partial \mathbf{f}_m(\mathbf{u})}{\partial x_m} = 0. \quad (1)$$

where $\mathbf{u}(\mathbf{x}, t) \in \mathbb{R}^n$ and $\mathbf{f}_m : \mathbb{R}^n \rightarrow \mathbb{R}^n$. We assume that (1) admits one or more entropy inequalities of the form

$$\frac{\partial S(\mathbf{u})}{\partial t} + \sum_{m=1}^d \frac{\partial F_m(\mathbf{u})}{\partial x_m} \leq 0, \quad F_m(\mathbf{u}) = \mathbf{v}(\mathbf{u})^T \mathbf{f}_m(\mathbf{u}) - \psi_m(\mathbf{u}), \quad (2)$$

where $S(\mathbf{u})$ is a scalar convex entropy, $F_m(\mathbf{u})$ are the associated entropy fluxes, ψ_m are the entropy potentials, and $\mathbf{v}(\mathbf{u})$ are the entropy variables

$$\mathbf{v}(\mathbf{u}) = \frac{\partial S}{\partial \mathbf{u}}.$$

Note that the convexity of $S(\mathbf{u})$ guarantees that the mapping between conservative and entropy variables is invertible.

For sufficiently regular solutions, one can derive the equality version of (2) by multiplying (1) by the entropy variables $\mathbf{v}(\mathbf{u})$. Applying the chain rule and properties of the entropy fluxes yields the corresponding entropy conservation condition. A vanishing viscosity argument yields the inequality version of (2) for more general classes of solutions [22, 33, 15]. This work utilizes an integrated cell version of (2) [45]. Consider a closed domain $D \subset \mathbb{R}^d$ with boundary ∂D . Then, integrating (2) over D and applying the divergence theorem yields

$$\int_D \frac{\partial S(\mathbf{u})}{\partial t} + \int_{\partial D} \sum_{m=1}^d (\mathbf{v}^T \mathbf{f}_m(\mathbf{u}) - \psi_m(\mathbf{u})) n_m \leq 0. \quad (3)$$

2.1. An intermediate entropy identity

We will enforce a version of the cell entropy inequality (3) by enforcing an intermediate identity. The derivation of the cell entropy inequality 3 starts by testing with the entropy variables $\mathbf{v}(\mathbf{u})$ and integrating over some domain D . Doing so and integrating the spatial derivative term by parts yields

$$\int_D \frac{\partial S(\mathbf{u})}{\partial t} + \sum_{m=1}^d \left[\int_D -\frac{\partial \mathbf{v}(\mathbf{u})}{\partial x_m} \mathbf{f}_m(\mathbf{u}) + \int_{\partial D} \mathbf{v}(\mathbf{u})^T \mathbf{f}_m(\mathbf{u}) n_m \right] = 0. \quad (4)$$

For a sufficiently regular solution \mathbf{u} , (3) becomes an entropy *equality*. Subtracting this equality from (4) yields

$$\sum_{m=1}^d \int_D -\frac{\partial \mathbf{v}}{\partial x_m}^T \mathbf{f}_m(\mathbf{u}) + \int_{\partial D} \psi_m(\mathbf{u}) n_m = 0. \quad (5)$$

For less regular solutions, (3) is an inequality. Subtracting (3) from (4) then yields

$$\sum_{m=1}^d \int_D -\frac{\partial \mathbf{v}}{\partial x_m}^T \mathbf{f}_m(\mathbf{u}) + \int_{\partial D} \psi_m(\mathbf{u}) n_m \geq 0. \quad (6)$$

We will add artificial viscosity such that we satisfy a discrete version of this inequality identity.

3. High order DG formulation

We assume that the domain $\Omega \subset \mathbb{R}^d$ is triangulated by non-overlapping simplicial elements D^k , where each element D^k is the image of a reference simplex \widehat{D} under some affine mapping $\phi^k : \widehat{D} \rightarrow D^k$. Let \mathbf{n} denote the outward normal vector $\mathbf{n} = [n_1, \dots, n_d]$ on each face of D^k . Finally, let $(u, v)_{D^k}, \langle u, v \rangle_{\partial D^k}$ denote the L^2 inner products on D^k and the surface ∂D^k

$$(u, v)_{D^k} \approx \int_{D^k} u(\mathbf{x})v(\mathbf{x}) \, dx, \quad \langle u, v \rangle_{\partial D^k} \approx \int_{\partial D^k} u(\mathbf{x})v(\mathbf{x}) \, dx,$$

where the approximate equality is due to the assumption that both volume and surface integrals in inner products are computed inexactly (e.g., approximated using quadrature).

We consider a standard DG formulation for an approximate solution \mathbf{u}_h on a single element D^k for (1) [47, 40]:

$$\left(\frac{\partial \mathbf{u}_h}{\partial t}, \mathbf{w} \right)_{D^k} + \sum_{m=1}^d \left(-\mathbf{f}_m(\mathbf{u}_h), \frac{\partial \mathbf{w}}{\partial x_m} \right)_{D^k} + \langle \mathbf{f}_n^*, \mathbf{w} \rangle_{\partial D^k} = \mathbf{0}, \quad \mathbf{w} \in [P^N(D^k)]^n, \quad (7)$$

where $P^N(D^k)$ denotes the space of total degree N polynomials on D^k . This formulation is derived by multiplying (1) by a test function $\mathbf{w} \in [P^N(D^k)]^n$, integrating by parts, and introducing a numerical flux \mathbf{f}_n^* across each inter-element interface. All volume and surface integrals are approximated using some quadrature rule, and summing up over all elements D^k yields a global DG formulation.

3.1. Semi-discrete entropy estimate

First, observe that the entropy variables $\mathbf{v}(\mathbf{u}_h)$ can be non-polynomial and do not (in general) lie in the test space $[P^N(D^k)]^n$. Thus, to derive a semi-discrete entropy estimate for (7), we must instead test with the L^2 projection of the entropy variables $\Pi_N \mathbf{v}(\mathbf{u}_h)$ [10]. Here, Π_N denotes the L^2 projection operator onto $P^N(D^k)$ such that for $f \in L^2(D^k)$

$$(\Pi_N f, v)_{D^k} = (f, v)_{D^k}, \quad \forall v \in P^N(D^k).$$

We note that similar observations on the non-polynomial nature of the entropy variables have been made by a variety of different groups in the literature [80, 31, 19, 13, 3].

Since $\frac{\partial \mathbf{u}_h}{\partial t} \in [P^N(D^k)]^n$ for method of lines discretizations, testing the time derivative term in (7) with the projected entropy variables yields

$$\left(\frac{\partial \mathbf{u}_h}{\partial t}, \Pi_N \mathbf{v}(\mathbf{u}_h) \right)_{D^k} = \left(\frac{\partial \mathbf{u}_h}{\partial t}, \mathbf{v}(\mathbf{u}_h) \right)_{D^k} = \left(\frac{\partial S(\mathbf{u}_h)}{\partial t}, 1 \right)_{D^k}, \quad (8)$$

where we have used the chain rule in time for the final step. Note that this equality still holds under inexact quadrature, so long as the L^2 projection operator Π_N is defined using the same inexact quadrature rule. We also note that these arguments are equivalent to the matrix-based arguments made in [10].

Using (8), we recover that the semi-discrete local rate of change of entropy over D^k is given by

$$\left(\frac{\partial S(\mathbf{u}_h)}{\partial t}, 1 \right)_{D^k} + \sum_{m=1}^d \left(-\mathbf{f}_m(\mathbf{u}_h), \frac{\partial \Pi_N \mathbf{v}(\mathbf{u}_h)}{\partial x_m} \right)_{D^k} + \langle \mathbf{f}_n^*, \Pi_N \mathbf{v}(\mathbf{u}_h) \rangle_{\partial D^k} = 0. \quad (9)$$

Unfortunately, (9) does not in general yield a semi-discrete entropy equality or inequality. At this point in the continuous derivation of either an entropy equality or inequality, the chain rule is typically used to manipulate the volume integral. However, due to the presence of the L^2 projection of the entropy variables $\Pi_N \mathbf{v}(\mathbf{u})$, we are unable to mimic this step. Moreover, because the integrals and inner products in this statement are typically discretized using inexact quadrature, the chain rule does not necessarily hold in spatially discrete settings.

High order entropy stable DG methods based on “flux differencing” [8, 30, 15, 21, 10] circumvent the loss of the chain rule by modifying the volume term in the DG formulation to incorporate non-dissipative numerical fluxes which satisfy an entropy conservation condition [75]. When combined with summation-by-parts (SBP) discretizations, this yields DG formulations which are semi-discretely entropy conservative or entropy stable in the sense that they satisfy a discrete version of the cell entropy identity (6), and thus a quadrature version of the cell entropy inequality (3)

$$\left(\frac{\partial S(\mathbf{u}_h)}{\partial t}, 1 \right)_{D^k} + \left\langle (\Pi_N \mathbf{v}(\mathbf{u}_h))^T \mathbf{f}_n^* - \sum_{m=1}^d \psi_m(\tilde{\mathbf{u}}) n_m, 1 \right\rangle_{\partial D^k} = 0.$$

where we have introduced the entropy projection $\tilde{\mathbf{u}}$:

$$\tilde{\mathbf{u}} = \mathbf{u} (\Pi_N \mathbf{v}(\mathbf{u}_h)), \quad (10)$$

e.g., the conservative variables evaluated in terms of the L^2 projection of the entropy variables.

Recent work has demonstrated that it is possible to enforce a cell entropy inequality outside of the “flux differencing” framework [53, 77]. In [53], a cell entropy inequality is enforced by solving a local knapsack problem to compute the optimal subcell blending of a standard high order nodal DG method with a compatible entropy stable low order scheme. In this paper, we add a minimal artificial viscosity to a standard high order DG method which is sufficient to recover an entropy inequality. The artificial viscosity coefficient is locally computable and relies on standard stability estimates for DG discretizations of viscous terms [29, 12].

4. Recovering an entropy inequality via artificial viscosity

We consider the following “monolithic” viscous regularization of (1)

$$\frac{\partial \mathbf{u}}{\partial t} + \sum_{m=1}^d \frac{\partial \mathbf{f}_m(\mathbf{u})}{\partial x_m} = \sum_{i,j=1}^d \frac{\partial}{\partial x_i} \left(\epsilon_k(\mathbf{u}) \frac{\partial \mathbf{u}}{\partial x_j} \right).$$

where $\epsilon_k(\mathbf{u}) \geq 0$. It is well known that it is possible to symmetrize many different viscous term by transforming to entropy variables [38, 43]. For the monolithic regularization, this can simply be done by applying the chain rule:

$$\frac{\partial \mathbf{u}}{\partial t} + \sum_{m=1}^d \frac{\partial \mathbf{f}_m(\mathbf{u})}{\partial x_m} = \sum_{i=1}^d \frac{\partial}{\partial x_i} \left(\epsilon_k(\mathbf{u}) \frac{\partial \mathbf{u}}{\partial \mathbf{v}} \frac{\partial \mathbf{v}}{\partial x_i} \right). \quad (11)$$

By the convexity of $S(\mathbf{u})$, the Jacobian matrix $\frac{\partial \mathbf{u}}{\partial \mathbf{v}}$ is symmetric and positive definite. We will analyze the slightly more general viscous regularization

$$\frac{\partial \mathbf{u}}{\partial t} + \sum_{m=1}^d \frac{\partial \mathbf{f}_m(\mathbf{u})}{\partial x_m} = \sum_{i,j=1}^d \frac{\partial}{\partial x_i} \left(\epsilon_k(\mathbf{u}) \mathbf{K}_{ij} \frac{\partial \mathbf{v}}{\partial x_j} \right). \quad (12)$$

where \mathbf{K}_{ij} denote blocks of a symmetric and positive semi-definite matrix \mathbf{K}

$$\mathbf{K} = \begin{bmatrix} \mathbf{K}_{11} & \dots & \mathbf{K}_{1d} \\ \vdots & \ddots & \vdots \\ \mathbf{K}_{d1} & \dots & \mathbf{K}_{dd} \end{bmatrix} = \mathbf{K}^T, \quad \mathbf{K} \succeq 0. \quad (13)$$

For example, taking $\mathbf{K}_{ij} = \delta_{ij} \frac{\partial \mathbf{u}}{\partial \mathbf{v}}$ recovers (11). Other viscous regularizations of (1) [43, 36, 74] can also be accommodated in this framework, but will not be the focus of this work.

4.1. DG formulation of artificial viscosity

We discretize (12) by adding a viscous contribution \mathbf{g}_{visc} to the DG formulation (7):

$$\left(\frac{\partial \mathbf{u}_h}{\partial t}, \mathbf{w} \right)_{D^k} + \sum_{m=1}^d \left(-\mathbf{f}_m(\mathbf{u}_h), \frac{\partial \mathbf{w}}{\partial x_m} \right)_{D^k} + \langle \mathbf{f}_n^*, \mathbf{w} \rangle_{\partial D^k} = (\mathbf{g}_{\text{visc}}, \mathbf{w})_{D^k}, \quad \mathbf{w} \in [P^N(D^k)]^n, \quad (14)$$

where the viscous terms \mathbf{g}_{visc} are discretizations of (12) using a BR-1 type discretization [12]. To simplify the notation, denote the L^2 projection of the entropy variables $\mathbf{v}_h = \Pi_N \mathbf{v}(\mathbf{u}_h)$. Then, \mathbf{g}_{visc} is given by the following formulation (where $i = 1, \dots, d$):

$$(\Theta_i, \mathbf{w}_{1,i})_{D^k} = \left(\frac{\partial \mathbf{v}_h}{\partial x_i}, \mathbf{w}_{1,i} \right)_{D^k} + \frac{1}{2} \langle \llbracket \mathbf{v}_h \rrbracket n_i, \mathbf{w}_{1,i} \rangle_{\partial D^k}, \quad \forall \mathbf{w}_{1,i} \in [P^N(D^k)]^n, \quad (15)$$

$$(\sigma_i, \mathbf{w}_{2,i})_{D^k} = \left(\sum_{j=1}^d \epsilon_k(\mathbf{u}_h) \mathbf{K}_{ij} \Theta_j, \mathbf{w}_{2,i} \right)_{D^k}, \quad \forall \mathbf{w}_{2,i} \in [P^N(D^k)]^n, \quad (16)$$

$$(\mathbf{g}_{\text{visc}}, \mathbf{w}_3)_{D^k} = \sum_{i=1}^d \left[\left(-\sigma_i, \frac{\partial \mathbf{w}_3}{\partial x_i} \right)_{D^k} + \langle \{\!\{ \sigma_i \}\!\} n_i, \mathbf{w}_3 \rangle_{\partial D^k} \right], \quad \forall \mathbf{w}_3 \in [P^N(D^k)]^n. \quad (17)$$

Here, $\llbracket \cdot \rrbracket$ and $\{\!\{ \cdot \}\!\}$ denote the jump and average operations:

$$\llbracket u \rrbracket = u^+ - u^-, \quad \{\!\{ u \}\!\} = \frac{1}{2} (u^+ + u^-),$$

where u^- denotes the interior value of u on a face of D^k , and u^+ denotes the exterior (neighboring) value of u across the same face. Here, Θ_i are DG approximations of derivatives of the entropy variables $\mathbf{v}(\mathbf{u}_h)$ with respect to the i th coordinate. In (16), we compute the viscous fluxes σ_i as the L^2 projection of $\sum_{j=1}^d \mathbf{K}_{ij} \Theta_j$ for $i = 1, \dots, d$ onto the approximation space of each element. The viscous terms \mathbf{g}_{visc} are the result of computing the divergence of the viscous fluxes in (17).

It can be shown using a straightforward modification of the proofs in [12] that the following stability estimate holds:

Lemma 1. (Adapted from Lemma 3.1 in [12]). Let \mathbf{g}_{visc} be given by (15), (16), (17). Then, for a periodic domain,

$$\sum_k -(\mathbf{g}_{\text{visc}}, \Pi_N \mathbf{v}(\mathbf{u}_h))_{D^k} = \sum_k \sum_{i,j=1}^d (\epsilon_k(\mathbf{u}_h) \mathbf{K}_{ij} \Theta_j, \Theta_i)_{D^k} \geq 0.$$

where $\Pi_N \mathbf{v}(\mathbf{u}_h)$ denotes the L^2 projection of the entropy variables.

Lemma 1 also holds under other appropriate impositions of boundary conditions; these will be treated in future work. We also note that Lemma 1 is agnostic to the regularity of $\epsilon_k(\mathbf{u}_h)$ and \mathbf{K}_{ij} ; in particular, they can be discontinuous from element to element. Because the estimate in Theorem 1 is localizable to each element, it is possible to determine exactly the amount of artificial viscosity necessary to satisfy a discrete version of the cell entropy identity (6)

$$\sum_{m=1}^d \left[\left(-\mathbf{f}_m(\mathbf{u}_h), \frac{\partial \Pi_N \mathbf{v}(\mathbf{u}_h)}{\partial x_m} \right)_{D^k} + \langle \psi_m(\tilde{\mathbf{u}}) n_m, 1 \rangle_{\partial D^k} \right] \geq 0. \quad (18)$$

where $\tilde{\mathbf{u}}$ is the entropy projection (10).

We first introduce the volume entropy residual $\delta_k(\mathbf{u}_h)$:

$$\delta_k(\mathbf{u}_h) = \sum_{m=1}^d \left[\left(-\mathbf{f}_m(\mathbf{u}_h), \frac{\partial \Pi_N \mathbf{v}(\mathbf{u}_h)}{\partial x_m} \right)_{D^k} + \langle \psi_m(\tilde{\mathbf{u}}) n_m, 1 \rangle_{\partial D^k} \right]. \quad (19)$$

Our goal will be to determine an artificial viscosity proportional to the violation of (18):

Lemma 2. Let $\epsilon_k(\mathbf{u}_h)$ on D^k satisfy

$$\sum_{i,j=1}^d (\epsilon_k(\mathbf{u}_h) \mathbf{K}_{ij} \Theta_j, \Theta_i)_{D^k} \geq -\min(0, \delta_k(\mathbf{u}_h)), \quad (20)$$

and let $\tilde{\mathbf{u}}$ denote the entropy projection (10). Then, (14) satisfies the following global entropy inequality:

$$\sum_k \left[\left(\frac{\partial S(\mathbf{u}_h)}{\partial t}, 1 \right)_{D^k} + \left\langle (\Pi_N \mathbf{v}(\mathbf{u}_h))^T \mathbf{f}_n^* - \sum_{m=1}^d \psi_m(\tilde{\mathbf{u}}) n_m, 1 \right\rangle_{\partial D^k} \right] \leq 0. \quad (21)$$

Proof. The inclusion of the viscous terms in (14) yields a slightly modified version of the semi-discrete entropy balance (9)

$$\left(\frac{\partial S(\mathbf{u}_h)}{\partial t}, 1 \right)_{D^k} + \sum_{m=1}^d \left(-\mathbf{f}_m(\mathbf{u}_h), \frac{\partial \Pi_N \mathbf{v}(\mathbf{u}_h)}{\partial x_m} \right)_{D^k} + \langle \mathbf{f}_n^*, \Pi_N \mathbf{v}(\mathbf{u}_h) \rangle_{\partial D^k} = (\mathbf{g}_{\text{visc}}, \Pi_N \mathbf{v}(\mathbf{u}_h))_{D^k}.$$

The result follows after summing the above estimate over all elements D^k and applying (22) and (1) to the resulting sum. \square

Remark 1. We note that it is possible to include additional semi-definite penalty terms involving the jumps of entropy variables in (17) [12]. We do not include them here for simplicity of presentation; however, because they add additional entropy dissipation to the sufficient condition (20), they can be incorporated without changing the main results of this paper. Moreover, the viscous discretization is not restricted to a BR-1 discretization; any viscous discretization which yields a localizable energy estimate results in the same semi-discrete entropy stability estimate in Lemma 2.

One can also derive a local entropy balance as is done in [72], though the cell entropy inequality will contain additional consistent terms resulting from the viscous discretization. Furthermore, if the numerical flux \mathbf{f}_n^* is entropy stable and evaluated using the entropy projection $\tilde{\mathbf{u}}$, then we have a global entropy inequality:

Lemma 3. Let the interface flux $\mathbf{f}_n^* = \mathbf{f}_n^*(\mathbf{u}_L, \mathbf{u}_R)$ be skew symmetric and entropy stable such that

$$\begin{aligned} (\mathbf{v}_L - \mathbf{v}_R)^T \mathbf{f}_n^*(\mathbf{u}_L, \mathbf{u}_R) &\leq \sum_{m=1}^d (\psi_m(\mathbf{u}_L) - \psi_m(\mathbf{u}_R)) n_m \\ \mathbf{f}_n^*(\mathbf{u}_L, \mathbf{u}_R) &= -\mathbf{f}_n^*(\mathbf{u}_R, \mathbf{u}_L). \end{aligned}$$

where $\mathbf{v}_L = \mathbf{v}(\mathbf{u}_L)$, $\mathbf{v}_R = \mathbf{v}(\mathbf{u}_R)$ are the entropy variables corresponding to the left and right solution states $\mathbf{u}_L, \mathbf{u}_R$. Then, if the interface flux is evaluated in terms of the entropy projection $\mathbf{f}_n^* = \mathbf{f}_n^*(\tilde{\mathbf{u}}^+, \tilde{\mathbf{u}})$, (21) implies the global entropy inequality

$$\left(\frac{\partial S(\mathbf{u}_h)}{\partial t}, 1 \right)_{\Omega} + \left\langle (\Pi_N \mathbf{v}(\mathbf{u}_h))^T \mathbf{f}_n^* - \sum_{m=1}^d \psi_m(\tilde{\mathbf{u}}) n_m, 1 \right\rangle_{\partial \Omega} \leq 0.$$

Proof. The proof is identical to the proof of the global entropy inequality in [15, 10]. We repeat it for completeness here. Since the sum over the interface terms in (21) includes all elements, each face f between element D^k and its neighbor $D^{k,+}$ yields two contributions:

$$\begin{aligned} & \int_{f \cap D^k} (\Pi_N \mathbf{v}(\mathbf{u}_h)) \cdot \mathbf{f}_n^*(\tilde{\mathbf{u}}^+, \tilde{\mathbf{u}}) - \sum_{m=1}^d \psi_m(\tilde{\mathbf{u}}) n_m \\ & + \int_{f \cap D^{k,+}} (\Pi_N \mathbf{v}(\mathbf{u}_h))^+ \cdot \mathbf{f}_{n^+}^*(\tilde{\mathbf{u}}, \tilde{\mathbf{u}}^+) - \sum_{m=1}^d \psi_m(\tilde{\mathbf{u}}^+) n_m^+ \end{aligned}$$

The global entropy inequality follows if the sums of these inter-element contributions are non-negative. Noting that $\mathbf{n}^+ = -\mathbf{n}$ and using the skew-symmetry property, we can combine like terms. Then, using the entropy stability of \mathbf{f}_n^* and that that $\tilde{\mathbf{u}} = \mathbf{v}(\Pi_N \mathbf{v}(\mathbf{u}_h))$, we conclude that

$$\int_f - \left((\Pi_N \mathbf{v}(\mathbf{u}_h))^+ - \Pi_N \mathbf{v}(\mathbf{u}_h) \right) \cdot \mathbf{f}_n^*(\tilde{\mathbf{u}}^+, \tilde{\mathbf{u}}) + \sum_{m=1}^d (\psi_m(\tilde{\mathbf{u}}^+) - \psi_m(\tilde{\mathbf{u}})) n_m \geq 0.$$

□

Note that, for periodic domains, the boundary contribution in Lemma 3 will also vanish.

Remark 2. While the global entropy inequality in Lemma 3 is exactly the same as the one satisfied by flux differencing entropy stable high order DG methods (see Theorem 3.4 of [15] or equation (87) in [10]), we note that flux differencing entropy stable high order DG methods are less entropy dissipative, since they satisfy an equality version of (21).

4.2. A piecewise constant viscosity coefficient

We now seek to derive an expression for $\epsilon_k(\mathbf{u}_h)$. The simplest approach for determining $\epsilon_k(\mathbf{u}_h)$ is to assume it is constant over each element; then, we can determine the smallest value of $\epsilon_k(\mathbf{u}_h)$ necessary to enforce an entropy inequality as follows:

$$\epsilon_k(\mathbf{u}_h) \geq \frac{-\min(0, \delta_k(\mathbf{u}_h))}{\sum_{i,j=1}^d (\mathbf{K}_{ij} \Theta_j, \Theta_i)_{D^k}}, \quad (22)$$

where $\delta_k(\mathbf{u}_h)$ is the volume entropy residual given by (19).

Remark 3. The denominator in (22) can be arbitrarily close to zero if \mathbf{u}_h is close to a constant. To avoid dividing by very small numbers, we approximate ratios of the form $\frac{a}{b}$ by

$$\frac{a}{b} \approx \frac{ab}{\delta + b^2}$$

where $\delta = 10^{-14}$ in all numerical experiments. This enforces that, if the solution approaches a constant and the denominator vanishes, the artificial viscosity parameter (22) approaches zero. This is consistent since a constant solution over an element automatically satisfies the discrete entropy identity (18).

Remark 4. *The viscous matrices \mathbf{K}_{ij} are functions of the conservative or entropy variables; however, these matrices can be evaluated at any admissible solution state while still retaining entropy stability. A computationally attractive option is to evaluate the viscous matrices using the local solution average $\bar{\mathbf{u}}_h$ as done in [26], which results in an element-wise constant \mathbf{K}_{ij} . This allows for the use of more efficient quadrature-free formulations [40, 9] when evaluating the viscous terms.*

Remark 5. *It was observed in [4, 35, 48] that artificial viscosities with continuous coefficients resulted in higher quality solutions compared with artificial viscosities with discontinuous coefficients. While we note that the artificial viscosity formulation used in this paper is stable and accurate even for discontinuous coefficients, users may smooth the locally computed $\epsilon_k(\mathbf{u}_h)$ without losing entropy stability. For example, one could construct C^0 viscosity coefficient whose value at vertices is the maximum of $\epsilon_k(\mathbf{u}_h)$ over all adjacent elements [48]. Interpolating these vertex values using P^1 or Q^1 elements would produce a new piecewise continuous viscosity coefficient which is pointwise greater than $\epsilon_k(\mathbf{u}_h)$ and thus would retain entropy stability. However, this interpolated C^0 viscosity yielded more dissipative solutions without improving accuracy in numerical experiments, so we do not include it in this work.*

We note that it is also possible to derive explicit expressions for a minimum norm artificial viscosity coefficient $\epsilon_k(\mathbf{u}_h)$ which varies at a subcell level within an element D^k . This is described in more detail along with numerical examples in Appendix B.

4.3. Simplification of the entropy projection under nodal collocation

Proving entropy stability using the artificial viscosity approach in this paper requires one non-standard ingredient in the DG discretization: the entropy projection (10). Recall that Lemma 3 requires that surface numerical fluxes be evaluated using the entropy projection in order to guarantee that the interface contributions in (21) are entropy dissipative. However, for nodal collocation DG methods, this additional entropy projection step is not necessary.

For collocation methods, quadrature points are collocated with interpolation points. It can be shown that the L^2 projection operator $\Pi_N = I_N$, where I_N denotes the degree N nodal interpolation operator [10]. Because the mapping between conservative and entropy variables is invertible, this implies that the values of $\tilde{\mathbf{u}}$ at nodal points is simply

$$\tilde{\mathbf{u}}(\mathbf{x}_i) = \mathbf{u} (I_N \mathbf{v}(\mathbf{u}_h)|_{\mathbf{x}=\mathbf{x}_i}) = \mathbf{u}(\mathbf{v}(\mathbf{u}_h(\mathbf{x}_i))) = \mathbf{u}_h(\mathbf{x}_i).$$

such that the entropy projection at quadrature/interpolation points reduces to the evaluation of the local polynomial solution \mathbf{u}_h . If the surface quadrature points are a subset of the collocated volume quadrature points (as is the case for the DG spectral element method, or DGSEM [49]), then the evaluation of the entropy projection at surface quadrature points reduces to the evaluation of the solution \mathbf{u}_h at those points as well. A similar structure holds under diagonal-norm nodal SBP discretizations on simplicial elements [15, 21].

4.4. Estimates for the volume entropy residual

We wish to estimate the magnitude of the volume entropy residual $\delta_k(\mathbf{u}_h)$, which turns out to enjoy a super-convergence property. We first assume exact integration for the proofs in this section, and discuss the effects of inexact quadrature in Section 4.4.1.

Lemma 4. For $\mathbf{u}_h \in [P^N D^k]^d$, the volume entropy residual $\delta_k(\mathbf{u}_h)$ (19) satisfies

$$\begin{aligned} \delta_k(\mathbf{u}_h) &= \int_{D^k} -\frac{\partial \Pi_N \mathbf{v}(\mathbf{u}_h)}{\partial x_m} \mathbf{f}_m(\mathbf{u}_h) + \int_{\partial D^k} \psi_m(\tilde{\mathbf{u}}) n_m = \\ &= \int_{D^k} \left(\bar{\mathbf{A}}_m \frac{\partial \Pi_N \mathbf{v}(\mathbf{u}_h)}{\partial x_m} - \Pi_N \left(\bar{\mathbf{A}}_m \frac{\partial \Pi_N \mathbf{v}(\mathbf{u}_h)}{\partial x_m} \right) \right)^T (\Pi_N \mathbf{v}(\mathbf{u}_h) - \mathbf{v}(\mathbf{u}_h)) \end{aligned} \quad (23)$$

for $m = 1, \dots, d$, where $\bar{\mathbf{A}}_m \approx \frac{\partial \mathbf{u}^T}{\partial \mathbf{v}} \frac{\partial \mathbf{f}_m}{\partial \mathbf{u}}$ is an appropriate mean value matrix, such as the Volpert or symmetric mean value matrix [5].

Proof. Since \mathbf{u}_h is sufficiently regular, the equality version of the entropy identity (5) holds under exact integration since $\tilde{\mathbf{u}} = \mathbf{u}(\Pi_N \mathbf{v}(\mathbf{u}_h))$

$$\int_{\partial D^k} \psi_m(\tilde{\mathbf{u}}) n_m = \int_{D^k} \frac{\partial \Pi_N \mathbf{v}(\mathbf{u}_h)}{\partial x_m} \mathbf{f}_m(\tilde{\mathbf{u}}). \quad (24)$$

Applying this to the left-hand side of (23) yields

$$\int_{D^k} -\frac{\partial \Pi_N \mathbf{v}(\mathbf{u}_h)}{\partial x_m} \mathbf{f}_m(\mathbf{u}_h) + \int_{\partial D^k} \psi_m(\tilde{\mathbf{u}}) n_m = \int_{D^k} \frac{\partial \Pi_N \mathbf{v}(\mathbf{u}_h)}{\partial x_m} (\mathbf{f}_m(\tilde{\mathbf{u}}) - \mathbf{f}_m(\mathbf{u}_h)).$$

Since $\tilde{\mathbf{u}} = \mathbf{u}(\Pi_N \mathbf{v}(\mathbf{u}_h))$, the mean value theorem implies

$$\mathbf{f}_m(\tilde{\mathbf{u}}) - \mathbf{f}_m(\mathbf{u}_h) = \bar{\mathbf{A}}_m (\Pi_N \mathbf{v}(\mathbf{u}_h) - \mathbf{v}(\mathbf{u}_h)),$$

where $\bar{\mathbf{A}}_m = \bar{\mathbf{A}}_m^T$ is an appropriate mean value matrix corresponding to $\frac{\partial \mathbf{u}^T}{\partial \mathbf{v}} \frac{\partial \mathbf{f}_m}{\partial \mathbf{u}}$, such as the Volpert mean value matrix (see (64) and (65) of [5], as well as [80]). This yields that

$$\int_{D^k} \frac{\partial \Pi_N \mathbf{v}(\mathbf{u}_h)}{\partial x_m} (\mathbf{f}_m(\tilde{\mathbf{u}}) - \mathbf{f}_m(\mathbf{u}_h)) = \int_{D^k} \left(\bar{\mathbf{A}}_m \frac{\partial \Pi_N \mathbf{v}(\mathbf{u}_h)}{\partial x_m} \right)^T (\Pi_N \mathbf{v}(\mathbf{u}_h) - \mathbf{v}(\mathbf{u}_h)).$$

Finally, since $\Pi_N \mathbf{v}(\mathbf{u}_h) - \mathbf{v}(\mathbf{u}_h)$ is the L^2 projection error, it is orthogonal to any degree N polynomial. This implies that it is orthogonal to $\Pi_N \left(\bar{\mathbf{A}}_m \frac{\partial \Pi_N \mathbf{v}(\mathbf{u}_h)}{\partial x_m} \right)$; subtracting

$$\Pi_N \left(\bar{\mathbf{A}}_m \frac{\partial \Pi_N \mathbf{v}(\mathbf{u}_h)}{\partial x_m} \right)^T (\Pi_N \mathbf{v}(\mathbf{u}_h) - \mathbf{v}(\mathbf{u}_h)) = 0$$

completes the proof. \square

Applying the Cauchy-Schwarz inequality to (23) yields that

$$\begin{aligned} & \left| \int_{D^k} -\frac{\partial \Pi_N \mathbf{v}(\mathbf{u}_h)}{\partial x_m} \mathbf{f}_m(\mathbf{u}_h) + \int_{\partial D^k} \psi_m(\tilde{\mathbf{u}}) n_m \right| \leq \\ & \left\| \bar{\mathbf{A}}_m \frac{\partial \Pi_N \mathbf{v}(\mathbf{u}_h)}{\partial x_m} - \Pi_N \left(\bar{\mathbf{A}}_m \frac{\partial \Pi_N \mathbf{v}(\mathbf{u}_h)}{\partial x_m} \right) \right\|_{L^2(D^k)} \|\Pi_N \mathbf{v}(\mathbf{u}_h) - \mathbf{v}(\mathbf{u}_h)\|_{L^2(D^k)}. \end{aligned}$$

If \mathbf{u}_h is a high order approximation of a sufficiently regular solution \mathbf{u} and the entropy $S(\mathbf{u}_h)$ is convex and sufficiently regular (e.g., when density and internal energy are uniformly bounded away from zero for the compressible Euler equations) such that $\mathbf{v}(\mathbf{u})$ is also a sufficiently regular mapping, the volume entropy residual is

$$\delta_k(\mathbf{u}_h) = \int_{D^k} -\frac{\partial \Pi_N \mathbf{v}(\mathbf{u}_h)}{\partial x_m} \mathbf{f}_m(\mathbf{u}_h) + \int_{\partial D^k} \psi_m(\tilde{\mathbf{u}}) n_m = O(h^{2N+2+d})$$

in d dimensions using standard approximation estimates and a scaling argument. This result is a sharpening of Theorem 5.5 in [16] and consistency estimates in [26, 58].

Remark 6. *The symmetry of $\bar{\mathbf{A}}_m$ follows from the symmetry of the flux Jacobians under transformation to entropy variables [61, 33] and the definitions of the Volpert or symmetric mean value matrix [5]. However, the symmetry of $\bar{\mathbf{A}}_m$ is not necessary for the superconvergence result to hold.*

Remark 7. *The observation that (24) is satisfied exactly under exact integration implies that standard weak form DG with the entropy projection and an entropy stable interface flux is entropy stable up to the accuracy of the volume quadrature. This was first pointed out in [19].*

4.4.1. The effect of inexact quadrature

While we have assumed exact integration in the proof of Lemma 4, a similar estimate holds for a sufficiently accurate quadrature. Suppose that the volume quadrature is exact for polynomial integrands $f \in P^{M_{\text{vol}}}(D^k)$ and the surface quadrature is exact for polynomial integrands $f \in P^{M_{\text{surf}}}(\partial D^k)$. For example, approximating 1D volume integrals using an $(N+1)$ point Gauss quadrature rule would be exact for $f \in P^{2N+1}$, such that $M_{\text{vol}} = 2N+1$. Then, since $\frac{\partial \Pi_N \mathbf{v}(\mathbf{u}_h)}{\partial x_m} \in P^{N-1}(D^k)$, under sufficient regularity of \mathbf{f}_m and \mathbf{u}_h ,

$$\begin{aligned} \left| \left(\mathbf{f}_m(\tilde{\mathbf{u}}), \frac{\partial \Pi_N \mathbf{v}(\mathbf{u}_h)}{\partial x_m} \right) - \int_{D^k} \frac{\partial \Pi_N \mathbf{v}(\mathbf{u}_h)}{\partial x_m} \mathbf{f}_m(\tilde{\mathbf{u}}) \right| &= O(h^{M_{\text{vol}}+1+d}) \\ \left| \langle \psi_m(\tilde{\mathbf{u}}) n_m, 1 \rangle - \int_{\partial D^k} \psi_m(\tilde{\mathbf{u}}) n_m \right| &= O(h^{M_{\text{surf}}+d}) \end{aligned}$$

Thus, if $M_{\text{vol}} \geq 2N+1$ and $M_{\text{surf}} \geq 2N+2$, then the quadrature error is of the same order as the volume entropy residual estimate in Lemma 4. We note that these quadrature exactness conditions are one order higher than necessary to prove optimal rates of convergence in [42].

4.5. Spurious null space modes

Recall that the artificial viscosity (22) involves the ratio between the volume entropy residual and the viscous entropy dissipation on an element D^k :

$$\epsilon_k(\mathbf{u}_h) = \frac{\min(0, \delta_k(\mathbf{u}_h))}{\sum_{i,j=1}^d (\Theta_i, \mathbf{K}_{ij} \Theta_j)_{D^k}}.$$

We wish to control the magnitude of the artificial viscosity; if $\epsilon_k(\mathbf{u}_h)$ is too large, it can negatively impact the maximum stable time-step size. Thus, if the denominator approaches zero, the numerator should approach zero at the same rate or faster.

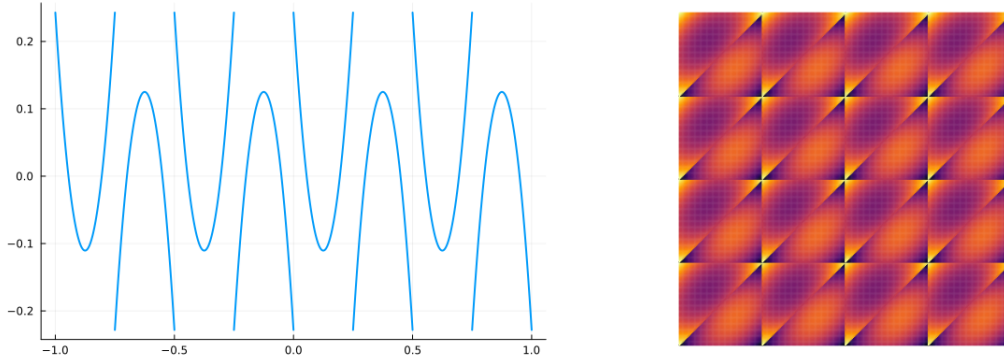


Figure 1: Examples of spurious null space modes of the BR-1 gradient in 1D and 2D.

Since Θ_i is a consistent approximation of $\frac{\partial \Pi_N \mathbf{v}(\mathbf{u}_h)}{\partial x_i}$, the denominator vanishes if the solution is constant. Luckily, the numerator (the volume entropy residual) also vanishes if the solution is constant, and numerical experiments suggest that the numerator converges to zero at the same rate or faster as \mathbf{u}_h approaches a constant. Unfortunately, for the BR-1 viscous discretization used in this work, spurious modes make it possible for the viscous entropy dissipation (the denominator) to be arbitrarily small compared to the volume entropy residual (the numerator).

The gradient Θ_i is approximated in (15) using a standard DG discretization of the gradient with a central flux. It is known that BR-1 discretizations of the Laplacian result in spurious non-constant null space eigenmodes [71, 40]. Discretizations of the gradient with a central flux (15) also admit similar spurious modes. such that applying (15) to such modes yields $\Theta_1, \dots, \Theta_d = \mathbf{0}$ [46]. Figure 1 illustrates examples of such modes for degree $N = 2$ approximations on uniform periodic meshes. While adding penalty terms to the divergence equation (17) suppresses such spurious eigenmodes for Laplacian and viscous flux derivatives [8, 12], they do not suppress spurious *gradient* modes.

These spurious modes do not appear to be a serious issue in practice when an upwind-like numerical flux is used for the convective discretization (7), as the jump penalization tends to rapidly dissipate away spurious modes [14]. We also note that non-central discretizations of the gradient, such as in the local DG method [18, 17], do not appear to produce spurious null space modes, and when combined with the artificial viscosity approach in this work, tend to produce smaller artificial viscosity coefficients. This will be analyzed in more detail in future work.

5. Comparison with other artificial viscosity methods

The literature on artificial viscosity is vast; even when restricting the literature review specifically to high order DG methods, there are hundreds of papers on artificial viscosity methods for nonlinear conservation laws. These artificial viscosity methods incorporate a variety of techniques, from modal and residual-based indicator methods to data-driven or machine-learning approaches [83, 63, 4, 48, 55, 60, 32, 23, 84, 85].

The artificial viscosity in this paper differs from many artificial viscosity methods in that the “indicator” $\epsilon_k(\mathbf{u}_h)$ is chosen to be the smallest cell-local value to guarantee an entropy inequality. As a result of this choice, the artificial viscosity in this paper *is not intended to damp spurious oscillations*. For example, when applied to the constant coefficient linear scalar advection equation,

the artificial viscosity coefficient $\epsilon_k(\mathbf{u}_h)$ vanishes, since the standard weak formulation of DG already satisfies a cell entropy inequality and the volume entropy residual $\delta_k(\mathbf{u}_h) = 0$. This behavior is contrast to artificial viscosity methods which are designed based on solution regularity or smoothness indicators. We note that it is straightforward to increase the magnitude of the artificial viscosity indicator $\epsilon_k(\mathbf{u}_h)$ if one wishes to damp spurious oscillations; however, the intent of the artificial viscosity in this work is to determine a *minimal* artificial viscosity which yields an entropy inequality.

The artificial viscosity method and choice of $\epsilon_k(\mathbf{u}_h)$ (22) are closely related to the “entropy residual” or “entropy commutator” indicators used in [34, 37], which are themselves a generalization of entropy viscosity and entropy residual methods [35, 86, 56]. The entropy commutator approach to entropy viscosity adds dissipation proportionally to the violation of the chain rule

$$\mathbf{v}(\mathbf{u}_h)^T \frac{\partial \mathbf{f}(\mathbf{u}_h)}{\partial x} - \frac{\partial F(\mathbf{u})}{\partial x} \approx 0, \quad F(\mathbf{u}) = \mathbf{v}(\mathbf{u}_h)^T \mathbf{f}(\mathbf{u}_h) - \psi(\mathbf{u}_h). \quad (25)$$

The approach taken in this work also adds dissipation proportional to the violation of (25), but with some distinctions. The magnitude of artificial viscosities (including entropy viscosity) typically depends on a heuristic normalization and scaling [50]. In contrast, once the viscosity model (e.g., the viscous matrices \mathbf{K}_{ij} and viscous DG formulation) are determined, there are no parameters to tune for the artificial viscosity used in this work. Moreover, in addition to using a P^1 continuous finite element approximation instead of a high order DG discretization, the entropy inequality in [34, 37] is approximately localized around the support of a single C^0 nodal basis function using Lagrange interpolation, while we localize the entropy inequality exactly using the L^2 projection of the entropy variables over a single DG element. Because the entropy stable artificial viscosity used in this work is proportional to the residual of an integrated version of (25) over each element, it could be interpreted as a “cell entropy viscosity”.

6. Numerical experiments

In this section, we present numerical experiments which confirm the robustness and accuracy of the proposed artificial viscosity method. All experiments are implemented in Julia using the `StartUpDG.jl` and `Trixi.jl` [69] libraries. Unless otherwise stated, all experiments utilize uniform meshes. In 1D, we investigate both nodal DGSEM formulations based on collocation at Legendre-Gauss-Lobatto nodes (referred to in figures as “nodal” DG discretizations), as well as degree N modal DG formulations based on an $(N + 2)$ point Gauss-Legendre quadrature rule (referred to in figures as “modal” DG discretizations). In 2D, we focus on total degree N approximations on triangular meshes, and utilize volume quadratures from [82] which are exact for degree $2N$ polynomials, as well as $(N + 1)$ point Gauss quadratures on faces.

For time integration, we utilize the `OrdinaryDiffEq.jl` library [64]. The adaptive 4-stage 3rd order strong stability preserving Runge-Kutta (SSPRK43) method [51, 20, 66] is used for all experiments. In 1D, the absolute and relative tolerance are set to $(10^{-8}, 10^{-6})$, and in 2D, we utilize absolute and relative tolerances of $(10^{-6}, 10^{-4})$.

6.1. Compressible Euler equations

All experiments are performed for the 1D and 2D compressible Euler equations, which are described below. Let \mathbf{u} denote the vector of conservative variables, which in 2D are

$$\mathbf{u} = \{\rho, \rho u_1, \dots, \rho u_d, E\} \in \mathbb{R}^{d+2}.$$

Here, ρ is density, u_i is the velocity in the i th coordinate direction, and E is the specific total energy. The pressure p is related to the conservative variables through the constitutive relations

$$p = (\gamma - 1)\rho e, \quad E = e + \frac{1}{2} \sum_{i=1}^d u_i^2,$$

where $\gamma = 1.4$ and e is the internal energy density. The compressible Euler equations in d dimensions are given by

$$\frac{\partial \mathbf{u}}{\partial t} + \sum_{i=1}^d \frac{\partial \mathbf{f}_i}{\partial x_i} = \mathbf{0}, \quad (26)$$

where \mathbf{f}_i denote the convective fluxes along the i th coordinate direction. For $d = 2$, the inviscid fluxes \mathbf{f}_i are given by

$$\mathbf{f}_1 = \begin{bmatrix} \rho u_1 \\ \rho u_1^2 + p \\ \rho u_1 u_2 \\ u_1(E + p) \end{bmatrix}, \quad \mathbf{f}_2 = \begin{bmatrix} \rho u_2 \\ \rho u_1 u_2 \\ \rho u_2^2 + p \\ u_2(E + p) \end{bmatrix}.$$

Setting velocity in either direction to zero recovers the 1D compressible Euler equations.

There exist an infinite family of convex entropies for the compressible Euler equations [38]; however, the compressible Navier-Stokes equations admit a mathematical entropy inequality with respect to only a single entropy function $S(\mathbf{u})$ and entropy potential $\psi_m(\mathbf{u})$

$$S(\mathbf{u}) = -\rho s, \quad \psi_m(\mathbf{u}) = \rho u_m,$$

where $s = \log\left(\frac{p}{\rho^\gamma}\right)$ denotes the physical entropy [43]. The derivative of the entropy with respect to the conservative variables yield the entropy variables $\mathbf{v}(\mathbf{u}) = \frac{\partial S}{\partial \mathbf{u}} = \{v_1, v_2, v_3, v_4\}$, where

$$v_1 = \frac{\rho e(\gamma + 1 - s) - E}{\rho e}, \quad v_{1+i} = \frac{\rho u_i}{\rho e}, \quad v_{d+2} = -\frac{\rho}{\rho e} \quad (27)$$

for $i = 1, \dots, d$. The inverse mapping is given by

$$\rho = -(\rho e)v_{d+2}, \quad \rho u_i = (\rho e)v_{1+i}, \quad E = (\rho e) \left(1 - \frac{\sum_{j=1}^d v_{1+j}^2}{2v_{d+2}} \right),$$

where $i = 1, \dots, d$, and ρe and s in terms of the entropy variables are

$$\rho e = \left(\frac{(\gamma - 1)}{(-v_{d+2})^\gamma} \right)^{1/(\gamma-1)} e^{\frac{-s}{\gamma-1}}, \quad s = \gamma - v_1 + \frac{\sum_{j=1}^d v_{1+j}^2}{2v_{d+2}}.$$

Finally, explicit expressions for the Jacobian matrix $\frac{\partial \mathbf{u}}{\partial \mathbf{v}}$ are given in [5] in terms of the sound speed a and specific total enthalpy H . In 2D, the Jacobian matrix is

$$\frac{\partial \mathbf{u}}{\partial \mathbf{v}} = \begin{bmatrix} \rho & \rho u_1 & \rho u_2 & E \\ \rho u_1^2 + p & \rho u_1 u_2 & u_1(E + p) & \\ & \rho u_2^2 + p & u_2(E + p) & \\ & & \rho H^2 - a^2 \frac{p}{\gamma-1} & \end{bmatrix},$$

$$a = \sqrt{\gamma \frac{p}{\rho}}, \quad H = \frac{a^2}{\gamma - 1} + \frac{1}{2}(u_1^2 + u_2^2),$$

where the lower triangular entries of $\frac{\partial \mathbf{u}}{\partial \mathbf{v}}$ are determined by symmetry.

h	$N = 1$	Rate	$N = 2$	Rate	$N = 3$	Rate	$N = 4$	Rate
1/2	5.735×10^{-1}		4.628×10^{-1}		4.058×10^{-1}		1.321×10^{-1}	
1/4	2.626×10^{-1}	1.13	8.553×10^{-2}	2.44	4.349×10^{-2}	3.22	1.297×10^{-2}	3.35
1/8	7.913×10^{-2}	1.73	1.713×10^{-2}	2.32	1.907×10^{-3}	4.51	3.425×10^{-4}	5.24
1/16	1.739×10^{-2}	2.19	3.035×10^{-3}	2.50	8.373×10^{-5}	4.51	1.016×10^{-5}	5.08
1/32	3.898×10^{-3}	2.16	3.663×10^{-4}	3.05	4.214×10^{-6}	4.31	3.230×10^{-7}	4.98

Table 1: Computed L^2 errors for the 2D density wave with amplitude $A = 0.5$ using an artificial viscosity-based entropy stable DG method.

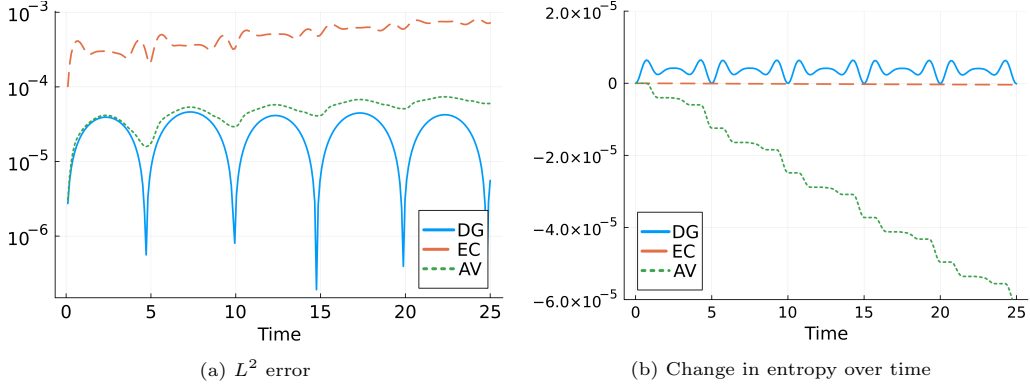


Figure 2: Evolution of L^2 error and entropy for the 1D density wave with amplitude $A = 0.5$. Here, “DG” refers to the standard DG method, “EC” refers to a flux differencing entropy stable DG method, and “AV” refers to the artificial viscosity-based entropy stable DG method.

6.2. Density wave and high order accuracy

We begin by examining the accuracy of the proposed discretization. We first consider the 2D density wave with amplitude $|A| < 1$:

$$\rho = 1 + A \sin(2\pi(x + y)), \quad u = .1, \quad v = .2, \quad p = 10.$$

We compute L^2 errors at final time $T = 1.7$ for amplitude $A = 0.5$ and show rates of convergence in Table 1. Optimal rates of convergence are observed for polynomial degrees $N = 1, \dots, 4$.

Next, we examine the behavior over time of the L^2 error over time for the 1D entropy wave with amplitude $|A| < 1$.

$$\rho = 1 + A \sin(2\pi x), \quad u = .1, \quad p = 10. \tag{28}$$

We consider both $A = 0.5$, where the minimum density is far from zero, and $A = 0.98$, where the minimum density is closer to zero. We evaluate errors for the standard nodal DG formulation, an artificial viscosity-based entropy stable nodal DG, and a flux differencing entropy stable nodal DG method using Ranocha’s entropy conservative volume flux [65].

Figures 2 and 3 shows plots of the L^2 errors and evolution of entropy up to time $T = 25$ for a degree $N = 7$ approximation over 4 elements. For $A = 0.5$, we observe that the L^2 errors are lowest for the standard nodal DG method, but that the errors for nodal DG with artificial viscosity hover just above the standard nodal DG error. In contrast, the errors for entropy stable flux differencing

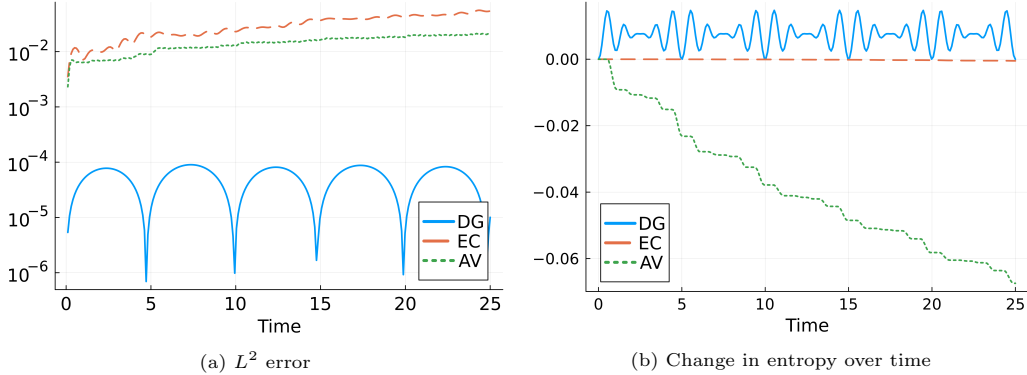


Figure 3: Evolution of L^2 error and entropy for the 1D density wave with amplitude $A = 0.98$. Here, “DG” refers to the standard DG method, “EC” refers to a flux differencing entropy stable DG method, and “AV” refers to the artificial viscosity-based entropy stable DG method.

	$N = 3, K = 8$	$N = 7, K = 4$
Flux differencing with EC flux	0.0613	0.1783
Entropy stable AV	0.0007	1.9239×10^{-5}
Standard weak form DG	3.6191×10^{-14}	6.323×10^{-14}

Table 2: Maximum real parts of the linearized spectra for nodal DG discretizations using a local Lax-Friedrichs interface flux.

nodal DG methods are about an order of magnitude larger. For $A = 0.98$, both flux differencing and artificial viscosity-based entropy stable nodal DG result in larger errors compared with standard nodal DG; however, the artificial viscosity-based entropy stable scheme results in smaller errors than the flux differencing entropy stable scheme. We also observe in both Figures 2 and 3 that the standard nodal DG scheme does not result in an entropy which is non-increasing in time.

Finally, we note that we observe similar patterns in the evolution of error and entropy over time when repeating the same 1D density wave experiment with $A = 0.5$ for a standard modal overintegrated DG scheme with $(N + 2)$ Gauss quadrature points. For $A = 0.98$, we observe that errors for the modal entropy stable schemes (both flux differencing and artificial viscosity-based) were larger in magnitude and resulted in a smaller maximum stable time-step size. We believe this to be due to the sensitivity of the entropy projection for near-vacuum states [13].

6.3. Linear stability for a well-resolved background flow

Flux differencing split form and entropy stable nodal DG methods are known to be less linearly stable than standard weak form nodal DG methods [27, 67]. In [27], the authors show that flux differencing with entropy conservative volume fluxes can be interpreted as adding potentially anti-diffusive correction to a linearly stable central scheme. It is known that a central volume flux recovers a standard nodal DG weak formulation [30], and since the approach taken in this work adds a small dissipative correction to a standard weak DG formulation, we expect the artificial viscosity approach in this paper to be more linearly stable than a split formulation.

We analyze the linear stability of a nodal DGSEM formulation by computing the spectral of the linearized Jacobian using automatic differentiation [70], where the background flow is given by the

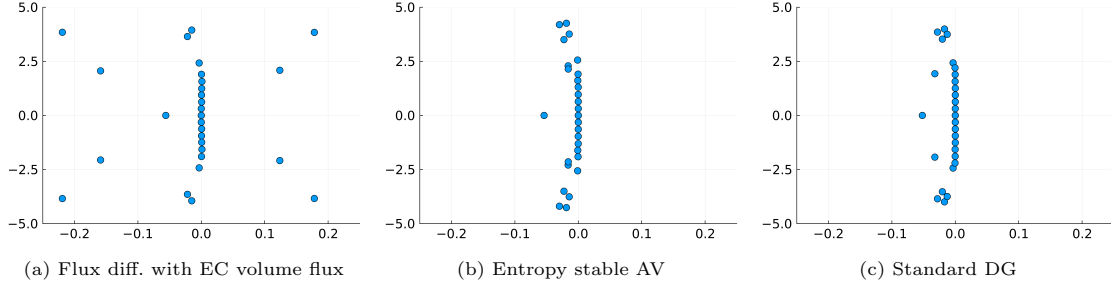


Figure 4: Spectra of the linearized Jacobian for a nodal DG discretization with $N = 7$, $K = 4$ and a local Lax-Friedrichs interface flux. The plots are zoomed near the origin to highlight the presence of eigenvalues with positive real parts.

1D density wave initial condition (28).¹ A local Lax-Friedrichs interface flux is used in all cases, and the entropy conservative flux of Ranocha [65] is used for the volume flux within the entropy stable flux differencing nodal DG discretization. Figure 4 shows a zoom near the origin of the spectra for degree $N = 3$ and a mesh of $K = 8$ uniform elements, as well as for degree $N = 7$ and a mesh of $K = 4$ uniform elements. Table 2 reports the computed maximum real part of the spectra, and we observe that entropy stable artificial viscosity reduces the maximum real part of the spectra by 2 to 6 orders of magnitude compared with an EC flux. However, neither method performs as well as standard weak form DG, which recovers a spectra with machine precision zero real parts.

We note that, for a flux differencing nodal DG method, the largest real part of the spectra appears to increase in magnitude as the minimum density decreases. This is not observed for either the standard weak DG formulation or for DG with entropy stability enforced via artificial viscosity.

6.4. Convergence of the artificial viscosity coefficients

Next, we examine the magnitude of the artificial viscosity coefficient $\epsilon_k(\mathbf{u}_h)$ for both smooth and discontinuous solution profiles. We compute artificial viscosity coefficients for the following smooth solution field

$$(\rho, u_1, u_2, p) = \left(1 + \frac{1}{2} \sin(0.1 + \pi x) \sin(0.2 + \pi y), \frac{1}{2} \sin(0.2 + \pi x) \sin(0.1 + \pi y), 0, \rho^\gamma \right)$$

and the following discontinuous solution field

$$(\rho, u_1, u_2, p) = \begin{cases} (1, 0, 0, 1) & |0.3x + y| < 0.5 \\ (2, .1, .2, 2^\gamma) & \text{otherwise.} \end{cases}$$

To compute the artificial viscosity coefficient, we compute the L^2 projection onto degree N polynomials of the conservative variables given by these solution fields, then determine the artificial

¹We also experimented with a modal DG formulation using an $(N + 2)$ point Gauss quadrature, but observed that the spectra included eigenvalues with large $O(100)$ positive real parts for the standard weak form DG scheme both with and without artificial viscosity. However, since the spectra does not provide a way to differentiate between standard weak form DG and the artificial viscosity presented in this work, we do not consider the results here.

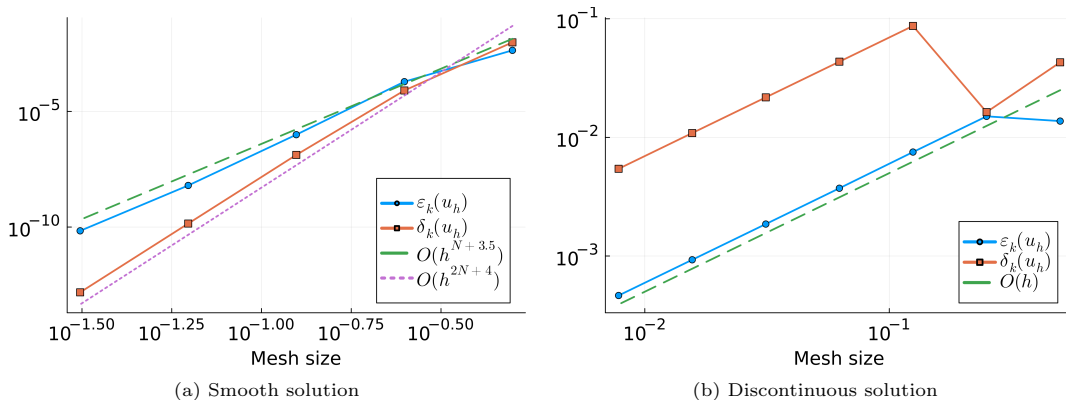


Figure 5: Convergence of the volume entropy residual $\delta_k(\mathbf{u}_h)$ (19) and the artificial viscosity coefficient $\epsilon_k(\mathbf{u}_h)$ (22) for fixed 2D smooth and discontinuous solution fields.

viscosity coefficient $\epsilon_k(\mathbf{u}_h)$ using (22). The quadrature is chosen based on the discussion in Section 4.4.1 such that the quadrature errors are of the same order of accuracy as the volume entropy residual. Specifically, we use a volume quadrature which is exact for degree $(2N + 1)$ polynomials, and the surface quadrature is taken to be an $(N + 2)$ point Gauss quadrature, which is sufficient to exactly integrate degree $(2N + 2)$ polynomials.

Figure 5 shows the maximum values of $\epsilon_k(\mathbf{u}_h)$ and $\delta_k(\mathbf{u}_h)$ (the volume entropy residual given by (19)) over degree $N = 3$ uniform triangular meshes. We observe that, for a smooth solution field, the volume entropy residual converges at the expected rate of $O(h^{2N+2+d})$, while the artificial viscosity coefficient converges at a rate of $O(h^{N+1.5+d})$. For a discontinuous solution field, we observe $O(h)$ convergence for both quantities once the mesh is sufficiently refined.

We note that, in practice, we use quadratures with lower degrees of exactness. We observe that, when taking the volume and surface quadratures to be exact for degree $2N$ and $2N + 1$ polynomials respectively, the volume entropy residual and artificial viscosity coefficient appear to achieve rates of $O(h^{2N+1+d})$ and $O(h^{N+0.5+d})$ for smooth solution fields, losing one order of convergence.

6.5. Modified Sod shock tube

Next, we consider the modified Sod shock tube problem [76] on the domain on $[0, 1]$

$$(\rho, u, p) = \begin{cases} (1, .75, 1) & x < 0.3 \\ (.125, 0, .1) & \text{otherwise.} \end{cases} \quad (29)$$

Figure 6 shows computed solutions at time $T = 0.2$ using both nodal [15] and modal [10, 11] flux differencing entropy stable DG methods, as well as both nodal and modal DG methods with entropy stability enforced via artificial viscosity. We note that the nodal and modal artificial viscosity-based entropy stable DG methods are similar except for the presence of a small solution artifact near the sonic point for the nodal DG method. This solution artifact decreases in magnitude under either mesh or degree refinement.

We observe that, while all methods produce spurious oscillations due to under-resolution of the shock, the oscillations present for the artificial viscosity-based entropy stable DG method are significantly smaller compared with the oscillations present for the flux differencing entropy stable

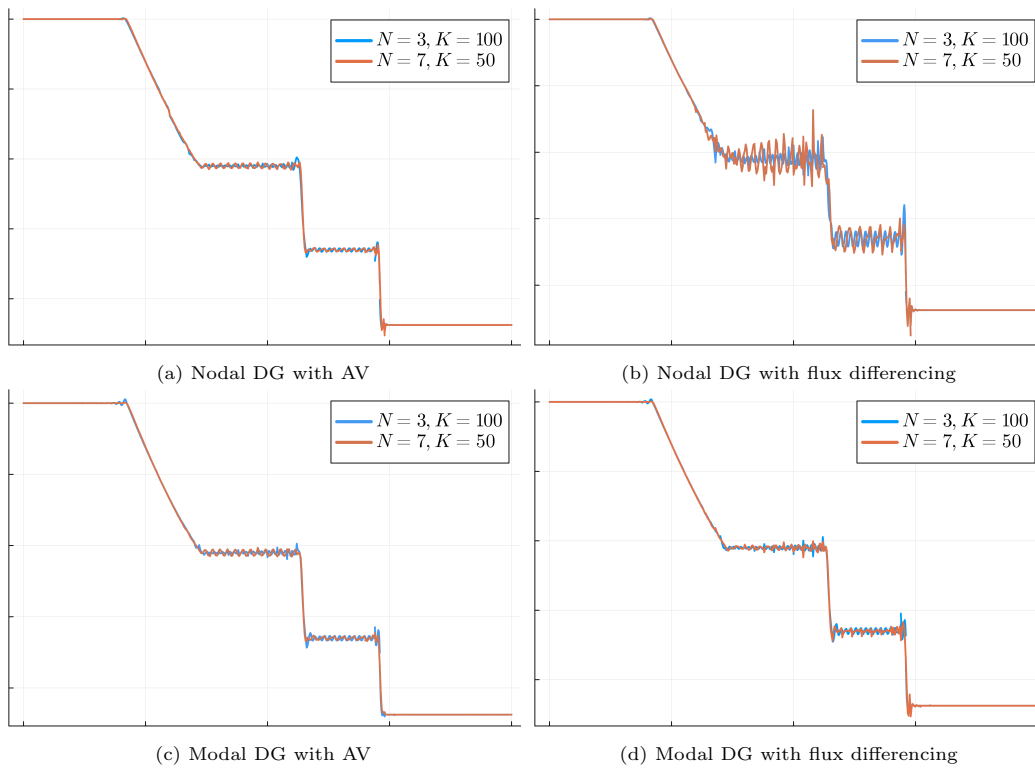


Figure 6: Comparison of entropy stable DG methods constructed using flux differencing and artificial viscosity.

nodal DG method. Moreover, the oscillations for the flux differencing entropy stable nodal DG methods increase in magnitude as the degree N increases, while the oscillations for flux differencing modal entropy stable DG method and the artificial viscosity-based entropy stable DG method remain about the same magnitude for both degrees $N = 3$ and $N = 7$. Using a contact-preserving entropy stable flux such as HLLC [6] or a Roe-type matrix dissipation [81, 79] reduces but does not eliminate such oscillations. Additional numerical results using contact-preserving interface fluxes are provided in Appendix A.1.

We note that there exist several additional techniques to suppress the spurious oscillations present in flux differencing entropy stable nodal DG methods. Earlier papers on high order entropy stable DG methods utilized a comparison principle, blending a standard DG method with an entropy stable DG method [8]. Shock capturing [39], bounds-preserving limiting [54], and heuristic artificial viscosity methods [59] have also been shown to be effective.

6.6. Shu-Osher problem

We consider the Shu-Osher sine-shock interaction problem [73] next, which is posed on the domain $[-5, 5]$ with initial condition

$$(\rho, u, p) = \begin{cases} (3.857143, 2.629369, 10.3333) & x < -4 \\ (1 + .2 \sin(5x), 0, 1) & x \geq -4. \end{cases}$$

We compare the computed DG solutions to a reference solution computed using 5th order WENO with 25000 cells. Figures 7, 8, and 9 show various entropy stable nodal and modal DG solutions for an under-resolved case (degree $N = 3$ with 50 elements), a more resolved moderate order case ($N = 3$ with 100 elements) and a more resolved high order case ($N = 7$ with 50 elements). Note that the $N = 7$, 50 element case results in the same total number of unknowns as the $N = 3$, 100 element case.

We observe that nodal flux differencing entropy stable schemes tend to produce solutions with significant spurious oscillations. These oscillations are significantly reduced for either modal flux differencing entropy stable DG schemes or artificial viscosity-based entropy stable DG schemes. We also observe that the artificial viscosity-based entropy stable DG results are slightly more diffusive than the modal flux differencing entropy stable DG results, as mentioned in Remark 2.

We also compare the number of timesteps taken by the adaptive SSPRK43 method for the specified tolerances. The nodal flux differencing entropy stable DG method required the fewest timesteps (15206). However, the method only remained stable for $N = 3$, and results in large magnitude spurious oscillations. The modal flux differencing entropy stable DG scheme contains significantly fewer spurious oscillations, and runs stably for both $N = 3$ and $N = 7$. However, the number of time-steps required is roughly double that of the nodal entropy stable DG scheme (35480 for $N = 3$ and 32793 for $N = 7$). Both the nodal and modal artificial viscosity schemes behaved similarly with respect to the number of timesteps; for $N = 3$, roughly 20k time-steps were required (21781 for nodal, 19741 for modal), while for $N = 7$, roughly 30k time-steps were required (30963 for nodal, 33119 for modal). We note that these results depend heavily on the tolerance and the choice of time-stepper; future work will analyze the maximum stable time-step restriction more rigorously.

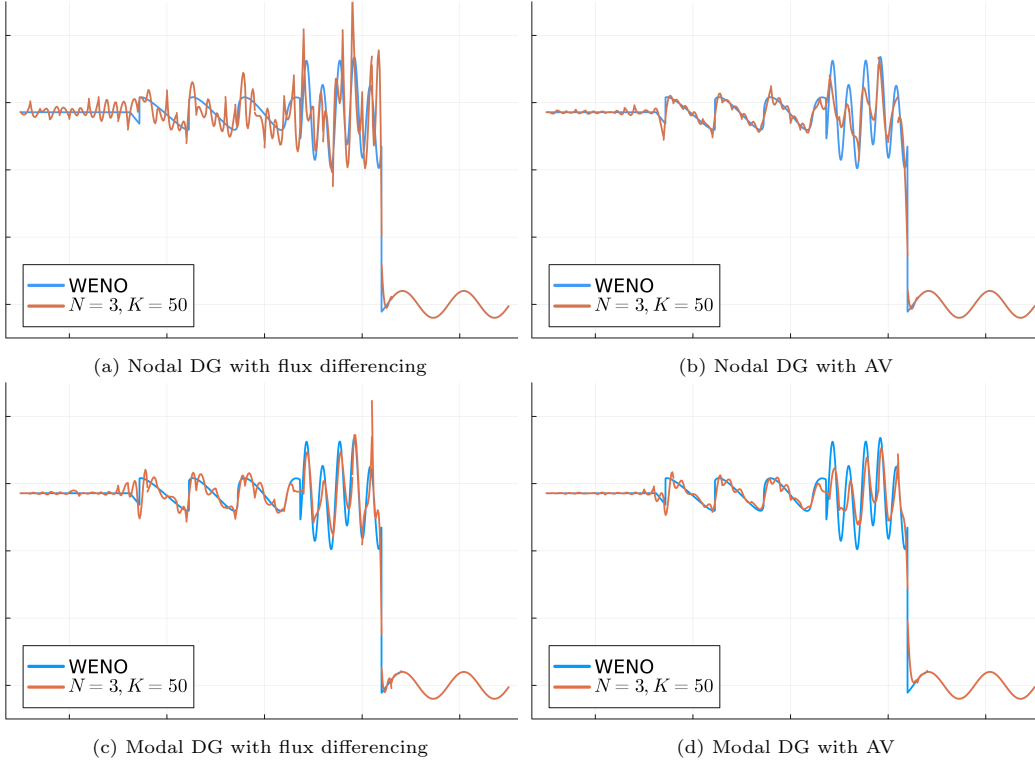


Figure 7: Entropy stable DG solutions of the Shu-Osher problem with $N = 3$, 50 elements.

6.7. A 2D Riemann problem

Next we consider a periodic version [10] of a 2D Riemann problem from [52]. The problem is posed on a periodic domain $[-1, 1]^2$ with initial condition

$$(\rho, u_1, u_2, p) = \begin{cases} (0.5313, 0, 0, 0.4) & x > 0, y > 0 \\ (1, 0.7276, 0, 1) & x < 0, y > 0 \\ (0.8, 0, 0, 1) & x < 0, y < 0 \\ (1, 0, 0.7276, 1) & x > 0, y < 0. \end{cases}$$

Figure 10 shows the density at final time $T = 0.25$, which we note looks very similar to the density computed by a modal flux differencing entropy stable DG method of the same degree and mesh resolution [10]. Figure 10 also shows a visualization of the viscosity coefficient $\epsilon_k(\mathbf{u}_h)$ given by (22). While the artificial viscosity coefficient appears to serve as an accurate troubled cell indicator, we emphasize that it was constructed only to replicate the entropy inequality satisfied by flux differencing entropy stable DG methods.

6.8. Long-time Kelvin-Helmholtz instability

We conclude with a long-time Kelvin-Helmholtz instability introduced in [13]. This example is run until final time $T = 25$ in order to develop pressure shocklets and small scale features resembling

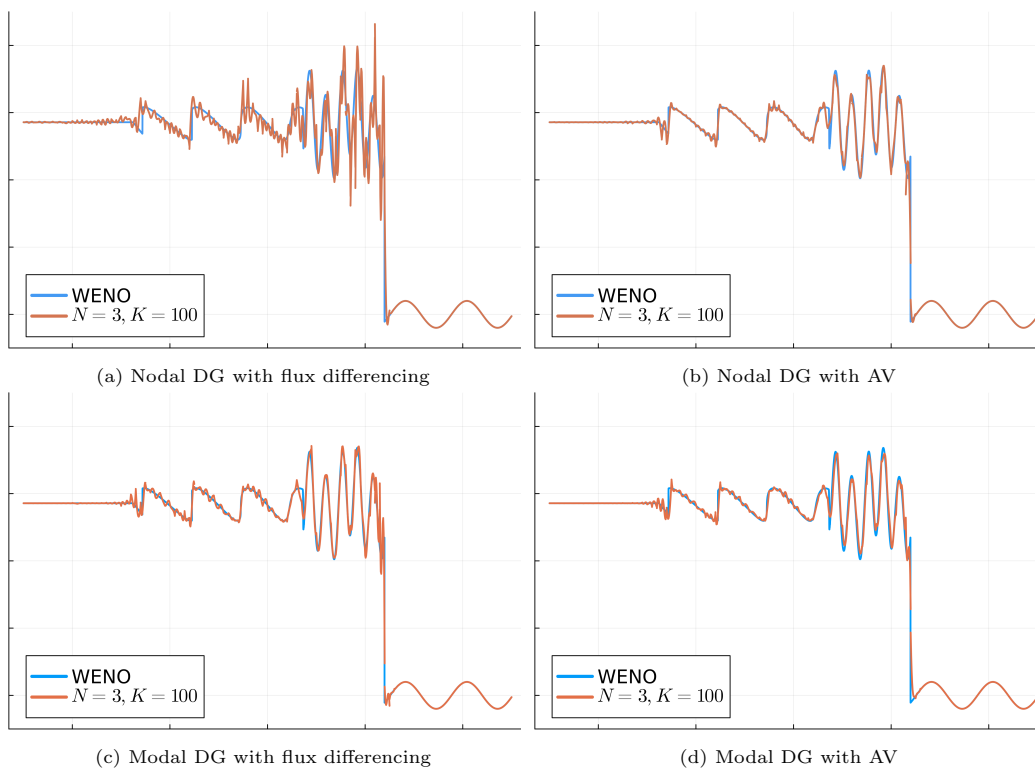


Figure 8: Entropy stable DG solutions of the Shu-Osher problem with $N = 3$, 100 elements.

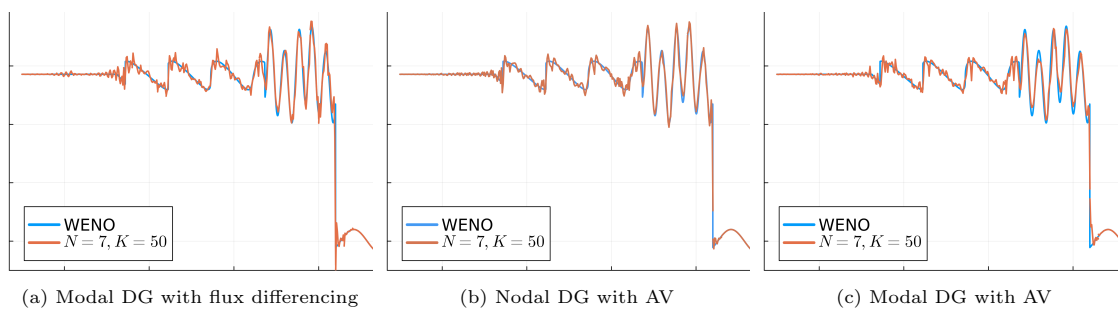


Figure 9: Entropy stable DG solutions of the Shu-Osher problem with $N = 7$, 50 elements. Results for nodal DG with flux differencing are not included as the simulation did not run to completion.

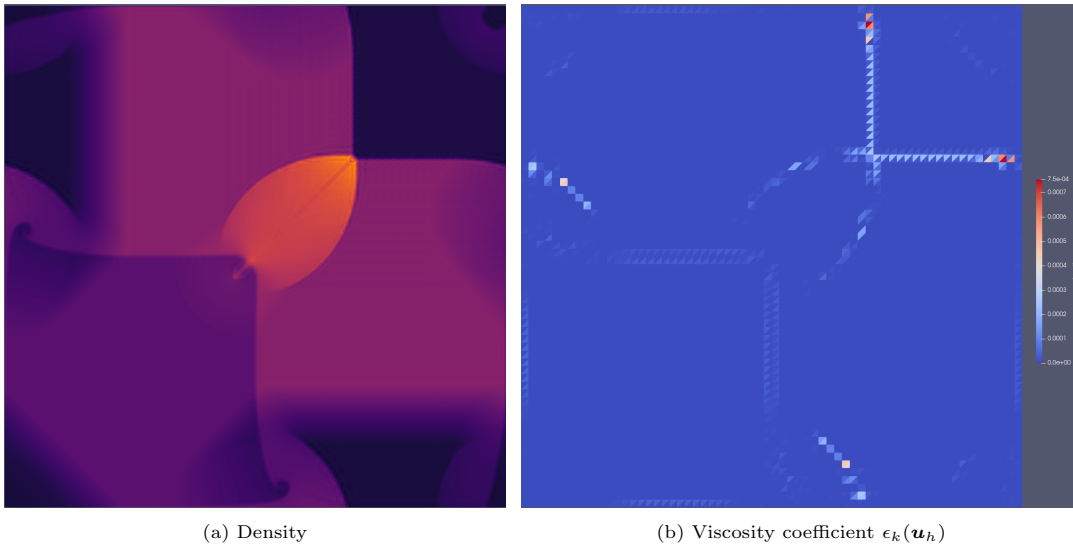


Figure 10: Solution of the 2D Riemann problem with degree $N = 3$ on a $64 \times 64 \times 2$ triangular mesh.

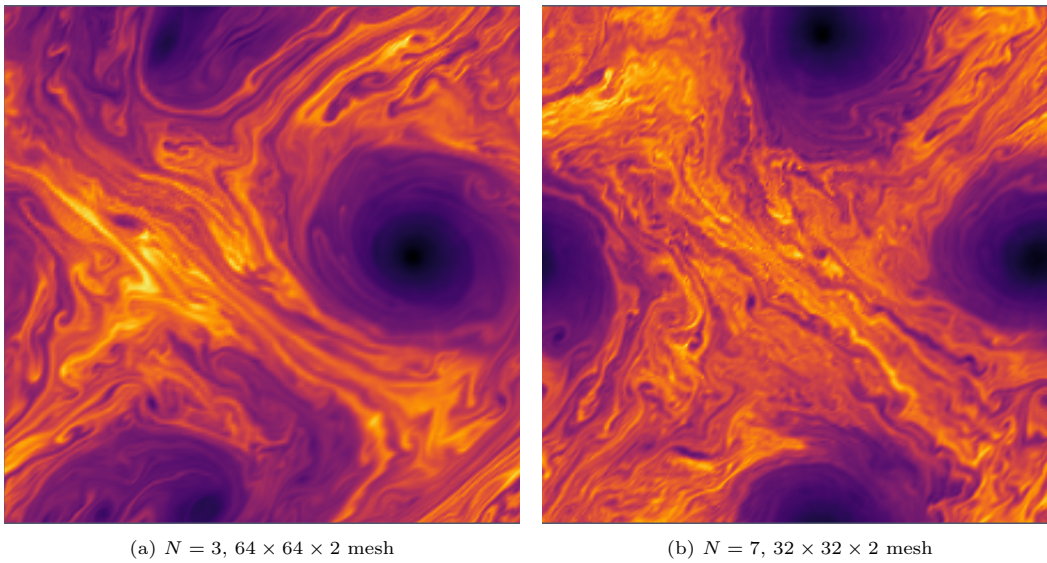


Figure 11: Solution of the 2D long-time Kelvin-Helmholtz instability using artificial viscosity-based entropy stable DG on triangular meshes.

turbulence. The initial condition is modified to add a small $O(1/100)$ non-symmetric scaling to the velocity in order to break symmetry. We note that, due to the lack of a viscous limit for the compressible Euler equations, numerical solutions to the Kelvin-Helmholtz instability depend strongly on discretization parameters [25] and do not converge to a unique solution under degree or mesh refinement. Thus, this test case should only be considered a test of robustness and a rough qualitative measure of how numerically dissipative a scheme is.

Figure 11 shows the solutions for both degree $N = 3$ and degree $N = 7$ solutions with roughly the same number of global degrees of freedom. As expected, the higher order approximation is able to resolve smaller scale features. Compared with the flux differencing entropy stable schemes in [13], the artificial viscosity-based schemes in this paper appear to be slightly more dissipative. However, as argued in [27], because of the lack of linear stability for flux differencing entropy stable schemes, it is not clear whether small scale structures present in a flux differencing entropy stable DG solution are physical or due to the introduction and evolution of non-physical numerical artifacts.

7. Conclusion

In this paper, we introduce an artificial viscosity-based method for recovering entropy stability for standard weak form DG discretizations. The artificial viscosity coefficients incorporate the error in a version of the volume entropy residual which utilizes the entropy projection. We prove that this estimate is super-convergent for sufficiently regular solutions and prove that, if interface fluxes are computed using the entropy projection, a standard DG method with this artificial viscosity satisfies the same global entropy inequality satisfied by flux differencing entropy stable DG methods.

Numerical experiments suggest that artificial viscosity-based entropy stable DG methods are slightly more dissipative than flux differencing entropy stable DG schemes. However, artificial viscosity-based entropy stable DG methods enjoy many of the same properties of flux differencing DG methods (such as robustness and high order accuracy), while also reducing spurious oscillations and improving linear stability.

The Julia codes used to generate the results in this paper are available at <https://github.com/jlchan/paper-artificial-viscosity-entropy-stable-2025>.

8. Acknowledgements

The authors gratefully acknowledge support from National Science Foundation under awards DMS-1943186 and DMS-223148. The authors also thank Alex Cicchino, Siva Nadarajah, Brian Christner, Raymond Park, Philipp Öffner, Lucas Wilcox, and Ayaboe Edoh for helpful discussions. The authors also acknowledge the Atum.jl library (<https://github.com/mwarusz/Atum.jl>), whose implementation of the matrix dissipation flux was used in this work [81, 79].

Appendix A. Additional 1D numerical experiments

In this section, we include some additional one-dimensional experiments.

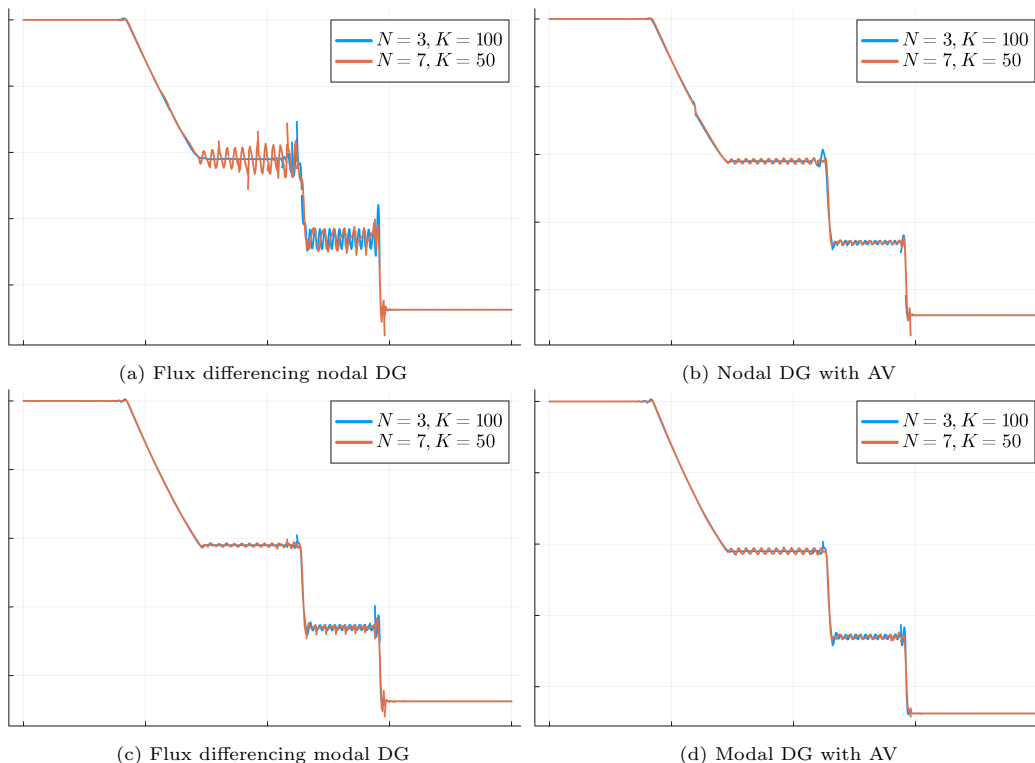


Figure A.12: Solutions of modified Sod with the HLLC interface flux.

Appendix A.1. Modified Sod with HLLC and Roe-type matrix dissipation interface fluxes

In addition to the local Lax-Friedrichs flux, we also experimented with HLLC interface fluxes [6] and interface fluxes based on Roe-type matrix dissipation [81, 79], both of which are contact-preserving. These contact preserving fluxes were also shown to improve the order of convergence for entropy stable nodal DG methods [41] and avoid spurious oscillations for flux differencing nodal DG methods applied to a variant of the original Sod shock tube [79].

Figure A.12 shows numerical results for the modified Sod problem using the HLLC flux (the matrix dissipation flux of [81, 79] produced very similar results). For degree $N = 3$, we observe that the use of HLLC and matrix dissipation fluxes reduce oscillations between the rarefaction wave and the contact discontinuity, but that they do not reduce oscillations between the contact discontinuity and shock. However, for $N = 7$, we do not observe a similar reduction in oscillations between the contact discontinuity and shock for either contact-preserving flux.

Appendix A.2. Modified Sod with smaller post-shock density and pressure

Next, we examined a version of modified Sod with smaller post-shock density and pressure, where we decreased the post-shock density and pressure by an additional factor of 10, such that $(\rho, u, p) = (.0125, 0, .01)$ for $x > 3$ in (29). For this initial condition, both nodal and modal flux differencing entropy stable DG methods crash before the final time of $T = 0.2$. Figure A.13 shows the resulting solution profile for nodal and modal artificial viscosity-enforced entropy stable DG.

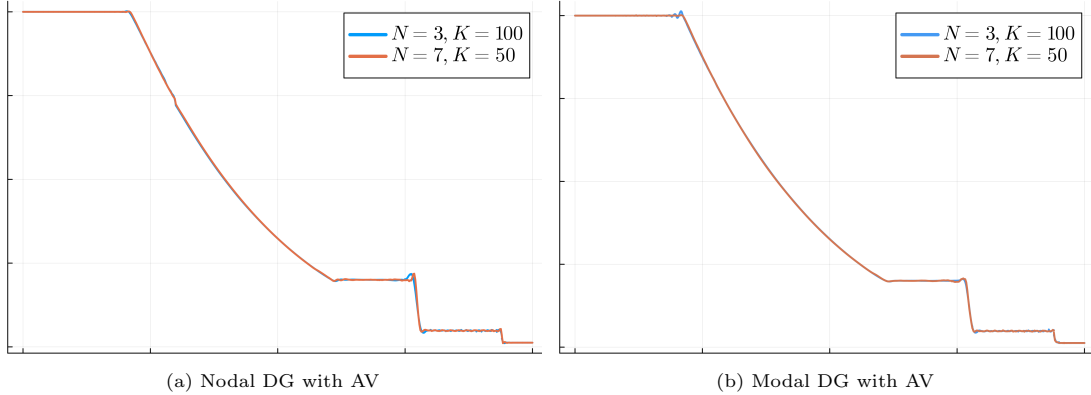


Figure A.13: Solutions of modified Sod with smaller post-shock density and pressure using standard DG with artificial viscosity-based entropy stability.

We note that the solution remains positive, despite the fact that for the modal DG discretization, the entropy projection (which is sensitive when density and pressure are small) is used to compute interface fluxes [13].

Finally, we note that for this version of modified Sod, the artificial viscosity near the shock was roughly $60\times$ larger than for the standard modified Sod problem (29). However, the number of time-steps taken by the adaptive time-stepper for this smaller density and pressure case only increased by a factor of ≈ 1.267 compared with the standard modified Sod initial condition (29), indicating that the magnitude of the artificial viscosity was not consistently large enough to induce a parabolic $O(h^2)$ maximum stable explicit time-step restriction.

Appendix A.3. Enforcing additional entropy inequalities

To demonstrate the impact of using the entropy projection $\tilde{\mathbf{u}}$ in the volume entropy residual (19), we compare a DG method where an additional entropy inequality is enforced. The second entropy inequality we enforce is the same as (19) except that the entropy potential ψ_m is evaluated at the DG solution \mathbf{u}_h rather than the entropy projection $\tilde{\mathbf{u}}$:

$$\sum_{m=1}^d \left[\left(-\mathbf{f}_m(\mathbf{u}_h), \frac{\partial \Pi_N \mathbf{v}(\mathbf{u}_h)}{\partial x_m} \right)_{D^k} + \langle \psi_m(\mathbf{u}_h) n_m, 1 \rangle_{\partial D^k} \right]. \quad (\text{A.1})$$

We note that we cannot use this modified entropy inequality on its own; enforcing only (A.1) results in unstable simulations where the adaptive time-step size converges to zero. However, we can enforce both entropy inequalities (19) and (A.1) by computing two artificial viscosity coefficients using (22) (one for each entropy inequality) and taking the maximum [35].

Figure A.14 shows the results of a degree $N = 3$ modal DG formulation under one and both of these entropy inequalities. We observe that enforcing the second entropy inequality without the entropy projection $\tilde{\mathbf{u}}$ results in a more diffusive solution. This is consistent with the fact that the volume entropy residual with the entropy projection (19) converges to zero at a faster rate than the volume entropy residual without entropy projection (A.1) based on estimates in [26]. Enforcing this additional entropy inequality also appears to provide some shock capturing effects, as oscillations around shocks are smoothed out.

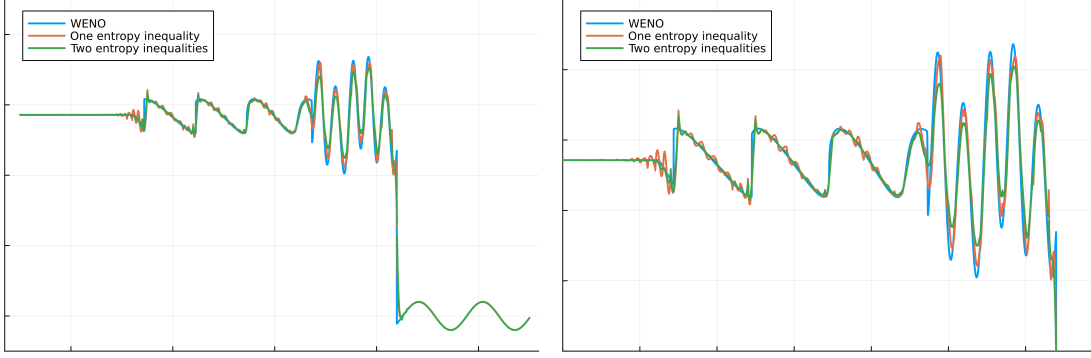


Figure A.14: Comparison of DG solutions (degree $N = 3$, 100 elements) to the Shu-Osher problem when enforcing one and two entropy inequalities.

Appendix B. A subcell version of the viscosity coefficient

If we wish to allow the local artificial viscosity coefficient $\epsilon_k(\mathbf{u}_h)$ to vary spatially within an element, we can determine an optimal choice for $\epsilon_k(\mathbf{u}_h)$ by minimizing the L^2 norm of $\epsilon_k(\mathbf{u}_h)$ subject to the entropy identity (20) and a non-negativity constraint. This optimization problem turns out to admit an analytical solution.

Lemma 5. *Let $\delta_k(\mathbf{u}_h)$ be the volume entropy residual (19). Consider the following inequality constrained optimization problem:*

$$\begin{aligned} \min_{\epsilon_k} \|\epsilon_k\|_{D^k}^2 \\ \sum_{i,j=1}^d (\epsilon_k \mathbf{K}_{ij} \Theta_j, \Theta_i)_{D^k} \geq -\min(0, \delta_k(\mathbf{u}_h)), \\ \epsilon_k(\mathbf{x}) \geq 0, \quad \forall \mathbf{x} \in D^k. \end{aligned}$$

This optimization problem has an explicit solution

$$\epsilon_k(\mathbf{u}_h) = -\min(0, \delta_k(\mathbf{u}_h)) \frac{a}{\|a\|_{D^k}^2}, \quad a(\mathbf{x}) = \sum_{i,j=1}^d \Theta_i^T \mathbf{K}_{ij} \Theta_j \geq 0. \quad (\text{B.1})$$

Proof. The optimization problem can be rewritten in a more abstract form:

$$\begin{aligned} \min_{\epsilon} \|\epsilon\|^2 \\ (a, \epsilon) \geq b \\ \epsilon \geq 0, \quad \forall \mathbf{x} \in D^k. \end{aligned} \quad (\text{B.2})$$

where $a(\mathbf{x}), b \geq 0$ and we have dropped the k, D^k subscripts for simplicity of notation. Note that $a(\mathbf{x}) = \sum_{i,j=1}^d \Theta_i^T \mathbf{K}_{ij} \Theta_j$ and $b = -\min(0, \delta_k(\mathbf{u}_h))$ recovers the optimization problem in Lemma 5.

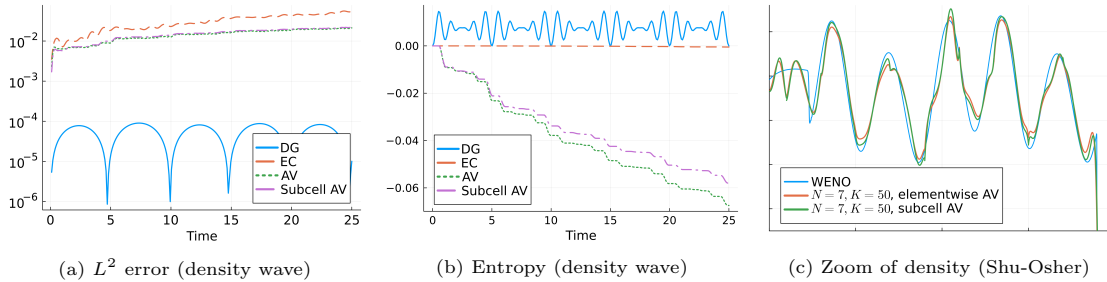


Figure B.15: Comparison of element-wise constant and subcell artificial viscosities for the 1D density wave and Shu-Osher problems using a degree $N = 7$ DG approximation.

Observe that if ϵ' satisfies $b \leq (a, \epsilon')$, then $b \leq (a, \epsilon') \leq \|a\| \|\epsilon'\|$ and $b/\|a\| \leq \|\epsilon'\|$. Thus, if we can find an $\epsilon \geq 0$ that meets the lower bound such that $\|\epsilon\| = b/\|a\|$, the solution is both feasible and optimal. One can verify that $\epsilon = b \frac{a}{\|a\|^2}$ satisfies both conditions. \square

Remark 8. We note that the proof of Lemma 5 implies that (B.2) is equivalent to an equality constrained minimum norm problem $\min_{\epsilon} \|\epsilon\|^2$ such that $(a, \epsilon) = b$.

Note that, if a is constant over an element, (B.1) reduces to the piecewise constant artificial viscosity coefficient in Section 4.2. To avoid division by small numbers, we again compute the ratio in (B.2) using the regularized ratio described in Remark 3.

Remark 9. We observe in numerical experiments that, even when using the subcell artificial viscosity $\epsilon_k(\mathbf{u}_h)$, evaluating the viscous matrices \mathbf{K}_{ij} at the average solution state as described in Remark 4 does not appear to degrade accuracy, results in a larger maximum stable time-step, and produces smaller spurious oscillations around shocks and under-resolved solution features. Thus, we assume that \mathbf{K}_{ij} is evaluated at averaged solution states $\bar{\mathbf{u}}_h$ for both the case when $\epsilon_k(\mathbf{u}_h)$ is piecewise constant and has subcell variations.

Despite the norm-minimizing nature of the subcell artificial viscosity, there does not appear to be a significant difference between the piecewise constant and subcell artificial viscosity coefficients in practice. Figure B.15 illustrates these differences for the 1D density wave (28) with amplitude $A = .98$ and the Shu-Osher sine-shock interaction problem. Both problems use degree $N = 7$; the density wave uses a mesh of 4 elements, while the Shu-Osher problem uses a mesh of 50 elements. The subcell artificial viscosity results in slightly less dissipative results for the density wave and the Shu-Osher problem. This effect becomes less pronounced for smaller polynomial degrees.

Appendix C. Comparison with local entropy correction terms

The artificial viscosity constructed in this work most closely resembles the entropy correction term of Abgrall, Öffner, and Ranocha [1, 2], which adds a similar dissipative term based on the zero-mean variation of the entropy variables over an element. More recent versions of this entropy correction term have both introduced the change of variables matrix $\mathbf{A}_0 = \frac{\partial \mathbf{u}}{\partial \mathbf{v}}$ as an inner product scaling and replaced the zero-mean variation term with the local derivative [26, 58].

Dropping inter-element coupling terms in the DG formulation of artificial viscosity results in a method that is similar to these local corrections, which are significantly simpler to implement.

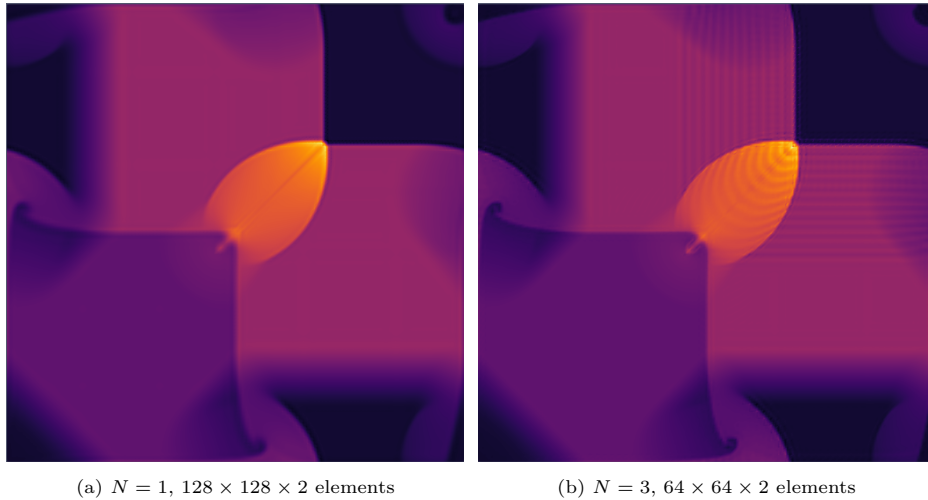


Figure C.16: Solutions to the 2D Riemann problem using a matrix-weighted version of Abgrall’s local entropy correction terms. The degree $N = 3$ solution contains numerical artifacts along the shock front.

However, we observed that adding only the local entropy correction term of [26, 58] was not sufficient to stabilize DG simulations of the 2D Riemann problem. Additionally, while the \mathbf{A}_0 -weighted variant of Abgrall, Öffner, and Ranocha’s correction term [2] successfully stabilizes the 2D Riemann problem, it also produces non-physical artifacts at higher orders of approximation. Figure C.16 shows the DG solution using the \mathbf{A}_0 -weighted version of the entropy correction in [2] where the entropy violation is estimated using the volume entropy residual (19). The degree $N = 3$ solution contains numerical artifacts along the shock front moving towards the upper-right hand corner, though these artifacts are not observed for the degree $N = 1$ solution.

References

- [1] Remi Abgrall. A general framework to construct schemes satisfying additional conservation relations. application to entropy conservative and entropy dissipative schemes. *Journal of Computational Physics*, 372:640–666, 2018.
- [2] Rémi Abgrall, Philipp Öffner, and Hendrik Ranocha. Reinterpretation and extension of entropy correction terms for residual distribution and discontinuous Galerkin schemes: application to structure preserving discretization. *Journal of Computational Physics*, 453:110955, 2022.
- [3] Boris D Andrews and Patrick E Farrell. High-order conservative and accurately dissipative numerical integrators via auxiliary variables. *arXiv preprint arXiv:2407.11904*, 2024.
- [4] Garrett E Barter and David L Darmofal. Shock capturing with PDE-based artificial viscosity for DGFEM: Part I. Formulation. *Journal of Computational Physics*, 229(5):1810–1827, 2010.
- [5] Timothy J Barth. Numerical methods for gasdynamic systems on unstructured meshes. In *An Introduction to Recent Developments in Theory and Numerics for Conservation Laws*:

Proceedings of the International School on Theory and Numerics for Conservation Laws, Freiburg/Littenweiler, October 20–24, 1997, pages 195–285. Springer, 1999.

- [6] Paul Batten, Nicholas Clarke, Claire Lambert, and Derek M Causon. On the choice of wavespeeds for the HLLC Riemann solver. *SIAM Journal on Scientific Computing*, 18(6):1553–1570, 1997.
- [7] Christophe Berthon, Manuel J Castro Díaz, Arnaud Duran, Tomás Morales de Luna, and Khaled Saleh. Artificial viscosity to get both robustness and discrete entropy inequalities. *Journal of Scientific Computing*, 97(3):65, 2023.
- [8] Mark H Carpenter, Travis C Fisher, Eric J Nielsen, and Steven H Frankel. Entropy stable spectral collocation schemes for the Navier-Stokes equations: Discontinuous interfaces. *SIAM Journal on Scientific Computing*, 36(5):B835–B867, 2014.
- [9] Jesse Chan. GPU-accelerated Bernstein–Bézier discontinuous Galerkin methods for wave problems. *SIAM Journal on Scientific Computing*, 39(2):A628–A654, 2017.
- [10] Jesse Chan. On discretely entropy conservative and entropy stable discontinuous Galerkin methods. *Journal of Computational Physics*, 362:346–374, 2018.
- [11] Jesse Chan. Skew-symmetric entropy stable modal discontinuous Galerkin formulations. *Journal of Scientific Computing*, 81(1):459–485, 2019.
- [12] Jesse Chan, Yimin Lin, and Tim Warburton. Entropy stable modal discontinuous Galerkin schemes and wall boundary conditions for the compressible Navier-Stokes equations. *Journal of Computational Physics*, 448:110723, 2022.
- [13] Jesse Chan, Hendrik Ranocha, Andrés M Rueda-Ramírez, Gregor Gassner, and Tim Warburton. On the entropy projection and the robustness of high order entropy stable discontinuous Galerkin schemes for under-resolved flows. *Frontiers in Physics*, 10:898028, 2022.
- [14] Jesse Chan and T Warburton. On the penalty stabilization mechanism for upwind discontinuous Galerkin formulations of first order hyperbolic systems. *Computers & Mathematics with Applications*, 74(12):3099–3110, 2017.
- [15] Tianheng Chen and Chi-Wang Shu. Entropy stable high order discontinuous Galerkin methods with suitable quadrature rules for hyperbolic conservation laws. *Journal of Computational Physics*, 345:427–461, 2017.
- [16] Tianheng Chen and Chi-Wang Shu. Review of entropy stable discontinuous Galerkin methods for systems of conservation laws on unstructured simplex meshes. *CSIAM Transactions on Applied Mathematics*, 1(1):1–52, 2020.
- [17] Bernardo Cockburn and Bo Dong. An analysis of the minimal dissipation local discontinuous Galerkin method for convection–diffusion problems. *Journal of Scientific Computing*, 32:233–262, 2007.
- [18] Bernardo Cockburn and Chi-Wang Shu. The local discontinuous Galerkin method for time-dependent convection-diffusion systems. *SIAM journal on numerical analysis*, 35(6):2440–2463, 1998.

- [19] Alessandro Colombo, Andrea Crivellini, and Alessandra Nigro. On the entropy conserving/stable implicit DG discretization of the Euler equations in entropy variables. *Computers & Fluids*, 232:105198, 2022.
- [20] Sidafa Conde, Imre Fekete, and John N Shadid. Embedded error estimation and adaptive step-size control for optimal explicit strong stability preserving Runge–Kutta methods. *arXiv preprint arXiv:1806.08693*, 2018.
- [21] Jared Crean, Jason E Hicken, David C Del Rey Fernández, David W Zingg, and Mark H Carpenter. Entropy-stable summation-by-parts discretization of the Euler equations on general curved elements. *Journal of Computational Physics*, 356:410–438, 2018.
- [22] Constantine M Dafermos and Constantine M Dafermos. *Hyperbolic conservation laws in continuum physics*, volume 3. Springer, 2005.
- [23] Niccolo Discacciati, Jan S Hesthaven, and Deep Ray. Controlling oscillations in high-order discontinuous Galerkin schemes using artificial viscosity tuned by neural networks. *Journal of Computational Physics*, 409:109304, 2020.
- [24] Ayaboe K Edoh. Conservative correction procedures utilizing artificial dissipation operators. *Journal of Computational Physics*, 504:112880, 2024.
- [25] Ulrik S Fjordholm, Roger Käppeli, Siddhartha Mishra, and Eitan Tadmor. Construction of approximate entropy measure-valued solutions for hyperbolic systems of conservation laws. *Foundations of Computational Mathematics*, 17(3):763–827, 2017.
- [26] Elena Gaburro, Philipp Öffner, Mario Ricchiuto, and Davide Torlo. High order entropy preserving ADER-DG schemes. *Applied Mathematics and Computation*, 440:127644, 2023.
- [27] Gregor J Gassner, Magnus Svärd, and Florian J Hindenlang. Stability issues of entropy-stable and/or split-form high-order schemes: Analysis of linear stability. *Journal of Scientific Computing*, 90:1–36, 2022.
- [28] Gregor J Gassner and Andrew R Winters. A novel robust strategy for discontinuous Galerkin methods in computational fluid mechanics: Why? When? What? Where? *Frontiers in Physics*, 8:500690, 2021.
- [29] Gregor J Gassner, Andrew R Winters, Florian J Hindenlang, and David A Kopriva. The BR1 scheme is stable for the compressible Navier–Stokes equations. *Journal of Scientific Computing*, 77(1):154–200, 2018.
- [30] Gregor J Gassner, Andrew R Winters, and David A Kopriva. Split form nodal discontinuous Galerkin schemes with summation-by-parts property for the compressible Euler equations. *Journal of Computational Physics*, 327:39–66, 2016.
- [31] Ioannis Gkanis and Charalambos Makridakis. A new class of entropy stable schemes for hyperbolic systems: Finite element methods. *Mathematics of Computation*, 90(330):1663–1699, 2021.
- [32] Jan Glaubitz, AC Nogueira, João LS Almeida, RF Cantão, and CAC Silva. Smooth and compactly supported viscous sub-cell shock capturing for discontinuous Galerkin methods. *Journal of Scientific Computing*, 79:249–272, 2019.

- [33] Edwige Godlewski and Pierre-Arnaud Raviart. *Numerical approximation of hyperbolic systems of conservation laws*, volume 118. Springer Science & Business Media, 2013.
- [34] Jean-Luc Guermond, Murtazo Nazarov, Bojan Popov, and Ignacio Tomas. Second-order invariant domain preserving approximation of the Euler equations using convex limiting. *SIAM Journal on Scientific Computing*, 40(5):A3211–A3239, 2018.
- [35] Jean-Luc Guermond, Richard Pasquetti, and Bojan Popov. Entropy viscosity method for nonlinear conservation laws. *Journal of Computational Physics*, 230(11):4248–4267, 2011.
- [36] Jean-Luc Guermond and Bojan Popov. Viscous regularization of the Euler equations and entropy principles. *SIAM Journal on Applied Mathematics*, 74(2):284–305, 2014.
- [37] Jean-Luc Guermond, Bojan Popov, and Ignacio Tomas. Invariant domain preserving discretization-independent schemes and convex limiting for hyperbolic systems. *Computer Methods in Applied Mechanics and Engineering*, 347:143–175, 2019.
- [38] Amiram Harten. On the symmetric form of systems of conservation laws with entropy. *Journal of computational physics*, 49, 1983.
- [39] Sebastian Hennemann, Andrés M Rueda-Ramírez, Florian J Hindenlang, and Gregor J Gassner. A provably entropy stable subcell shock capturing approach for high order split form DG for the compressible Euler equations. *Journal of Computational Physics*, 426:109935, 2021.
- [40] Jan S Hesthaven and Tim Warburton. *Nodal discontinuous Galerkin methods: algorithms, analysis, and applications*. Springer Science & Business Media, 2007.
- [41] Florian J Hindenlang and Gregor J Gassner. On the order reduction of entropy stable DGSEM for the compressible Euler equations. In *Spectral and High Order Methods for Partial Differential Equations ICOSAHOM 2018: Selected Papers from the ICOSAHOM Conference, London, UK, July 9-13, 2018*, pages 21–44. Springer International Publishing, 2020.
- [42] Juntao Huang and Chi-Wang Shu. Error estimates to smooth solutions of semi-discrete discontinuous Galerkin methods with quadrature rules for scalar conservation laws. *Numerical Methods for Partial Differential Equations*, 33(2):467–488, 2017.
- [43] Thomas JR Hughes, LP Franca, and M Mallet. A new finite element formulation for computational fluid dynamics: I. Symmetric forms of the compressible Euler and Navier-Stokes equations and the second law of thermodynamics. *Computer Methods in Applied Mechanics and Engineering*, 54(2):223–234, 1986.
- [44] S Jain and Parviz Moin. Stable, entropy-consistent, and localized artificial-viscosity method for capturing shocks and contact discontinuities. *Center for Turbulence Research Annual Research Briefs*, 2021, 2021.
- [45] Guang Shan Jiang and Chi-Wang Shu. On a cell entropy inequality for discontinuous Galerkin methods. *Mathematics of Computation*, 62(206):531–538, 1994.
- [46] Lorenz John, Michael Neilan, and Iain Smears. Stable discontinuous Galerkin FEM without penalty parameters. In *Numerical mathematics and advanced applications ENUMATH 2015*, pages 165–173. Springer, 2016.

- [47] George Karniadakis and Spencer J Sherwin. *Spectral/hp element methods for computational fluid dynamics*. Oxford University Press, USA, 2005.
- [48] Andreas Klöckner, Tim Warburton, and Jan S Hesthaven. Viscous shock capturing in a time-explicit discontinuous Galerkin method. *Mathematical Modelling of Natural Phenomena*, 6(3):57–83, 2011.
- [49] David A Kopriva and Gregor Gassner. On the quadrature and weak form choices in collocation type discontinuous Galerkin spectral element methods. *Journal of Scientific Computing*, 44:136–155, 2010.
- [50] Adeline Kornelus and Daniel Appelö. On the scaling of entropy viscosity in high order methods. In *Spectral and High Order Methods for Partial Differential Equations ICOSAHOM 2016: Selected Papers from the ICOSAHOM conference, June 27-July 1, 2016, Rio de Janeiro, Brazil*, pages 175–187. Springer, 2017.
- [51] Johannes Franciscus Bernardus Maria Kraaijevanger. Contractivity of Runge-Kutta methods. *BIT Numerical Mathematics*, 31(3):482–528, 1991.
- [52] Alexander Kurganov and Eitan Tadmor. Solution of two-dimensional Riemann problems for gas dynamics without Riemann problem solvers. *Numerical Methods for Partial Differential Equations: An International Journal*, 18(5):584–608, 2002.
- [53] Yimin Lin and Jesse Chan. High order entropy stable discontinuous Galerkin spectral element methods through subcell limiting. *Journal of Computational Physics*, 498:112677, 2024.
- [54] Yimin Lin, Jesse Chan, and Ignacio Tomas. A positivity preserving strategy for entropy stable discontinuous Galerkin discretizations of the compressible Euler and Navier-Stokes equations. *Journal of Computational Physics*, 475:111850, 2023.
- [55] Y Lv and M Ihme. Taming nonlinear instability for discontinuous galerkin scheme with artificial viscosity. *Center for Turbulence Research, Annual Research Briefs*, 2014.
- [56] Yu Lv, Yee Chee See, and Matthias Ihme. An entropy-residual shock detector for solving conservation laws using high-order discontinuous Galerkin methods. *Journal of Computational Physics*, 322:448–472, 2016.
- [57] Andrew Majda and Stanley Osher. Numerical viscosity and the entropy condition. *Communications on Pure and Applied Mathematics*, 32(6):797–838, 1979.
- [58] Yogiraj Mantri, Philipp Öffner, and Mario Ricchiuto. Fully well-balanced entropy controlled discontinuous Galerkin spectral element method for shallow water flows: global flux quadrature and cell entropy correction. *Journal of Computational Physics*, 498:112673, 2024.
- [59] Andrés Mateo-Gabín, Juan Manzanero, and Eusebio Valero. An entropy stable spectral vanishing viscosity for discontinuous Galerkin schemes: application to shock capturing and LES models. *Journal of Computational Physics*, 471:111618, 2022.
- [60] Craig Michoski, Clint Dawson, Ethan J Kubatko, Damrongsak Wirasaet, S Brus, and Joannes J Westerink. A comparison of artificial viscosity, limiters, and filters, for high order discontinuous Galerkin solutions in nonlinear settings. *Journal of Scientific Computing*, 66:406–434, 2016.

- [61] M.S Mock. Systems of conservation laws of mixed type. *Journal of Differential Equations*, 37(1):70–88, 1980.
- [62] Tristan Montoya and David W Zingg. Efficient entropy-stable discontinuous spectral-element methods using tensor-product summation-by-parts operators on triangles and tetrahedra. *Journal of Computational Physics*, 516:113360, 2024.
- [63] Per-Olof Persson and Jaime Peraire. Sub-cell shock capturing for discontinuous Galerkin methods. In *44th AIAA Aerospace Sciences Meeting and Exhibit*, page 112, 2006.
- [64] Christopher Rackauckas and Qing Nie. Differentialequations. jl—a performant and feature-rich ecosystem for solving differential equations in Julia. *Journal of open research software*, 5(1):15–15, 2017.
- [65] Hendrik Ranocha. Entropy conserving and kinetic energy preserving numerical methods for the Euler equations using summation-by-parts operators. *Spectral and high order methods for partial differential equations ICOSAHOM 2018*, 134:525–535, 2020.
- [66] Hendrik Ranocha, Lisandro Dalcin, Matteo Parsani, and David I Ketcheson. Optimized Runge-Kutta methods with automatic step size control for compressible computational fluid dynamics. *Communications on Applied Mathematics and Computation*, 4(4):1191–1228, 2022.
- [67] Hendrik Ranocha and Gregor J Gassner. Preventing pressure oscillations does not fix local linear stability issues of entropy-based split-form high-order schemes. *Communications on Applied Mathematics and Computation*, pages 1–24, 2021.
- [68] Hendrik Ranocha, Michael Schlottke-Lakemper, Jesse Chan, Andrés M Rueda-Ramírez, Andrew R Winters, Florian Hindenlang, and Gregor J Gassner. Efficient implementation of modern entropy stable and kinetic energy preserving discontinuous Galerkin methods for conservation laws. *ACM Transactions on Mathematical Software*, 49(4):1–30, 2023.
- [69] Hendrik Ranocha, Michael Schlottke-Lakemper, Andrew R Winters, Erik Faulhaber, Jesse Chan, and Gregor J Gassner. Adaptive numerical simulations with Trixi. jl: A case study of Julia for scientific computing. In *Proceedings of the JuliaCon Conferences*, volume 1, page 77, 2022.
- [70] Jarrett Revels, Miles Lubin, and Theodore Papamarkou. Forward-mode automatic differentiation in Julia. *arXiv preprint arXiv:1607.07892*, 2016.
- [71] SJ Sherwin, RM Kirby, J Peiró, RL Taylor, and OC Zienkiewicz. On 2D elliptic discontinuous Galerkin methods. *International journal for numerical methods in engineering*, 65(5):752–784, 2006.
- [72] Chi-Wang Shu. Discontinuous Galerkin methods: general approach and stability. *Numerical solutions of partial differential equations*, 201:149–201, 2009.
- [73] Chi-Wang Shu. High order weighted essentially nonoscillatory schemes for convection dominated problems. *SIAM review*, 51(1):82–126, 2009.
- [74] Magnus Svärd. Refining the diffusive compressible Euler model. *Physica A: Statistical Mechanics and its Applications*, 635:129474, 2024.

- [75] Eitan Tadmor. The numerical viscosity of entropy stable schemes for systems of conservation laws. I. *Mathematics of Computation*, 49(179):91–103, 1987.
- [76] Eleuterio F Toro. *Riemann solvers and numerical methods for fluid dynamics: a practical introduction*. Springer Science & Business Media, 2013.
- [77] François Vilar. Local subcell monolithic DG/FV convex property preserving scheme on unstructured grids and entropy consideration. *Journal of Computational Physics*, page 113535, 2024.
- [78] John VonNeumann and Robert D Richtmyer. A method for the numerical calculation of hydrodynamic shocks. *Journal of applied physics*, 21(3):232–237, 1950.
- [79] Maciej Waruszewski, Jeremy E Kozdon, Lucas C Wilcox, Thomas H Gibson, and Francis X Giraldo. Entropy stable discontinuous Galerkin methods for balance laws in non-conservative form: Applications to the Euler equations with gravity. *Journal of Computational Physics*, 468:111507, 2022.
- [80] David M Williams. An analysis of discontinuous Galerkin methods for the compressible Euler equations: entropy and L^2 stability. *Numerische Mathematik*, 141(4):1079–1120, 2019.
- [81] Andrew R Winters, Dominik Derigs, Gregor J Gassner, and Stefanie Walch. A uniquely defined entropy stable matrix dissipation operator for high Mach number ideal MHD and compressible Euler simulations. *Journal of Computational Physics*, 332:274–289, 2017.
- [82] Hong Xiao and Zydrunas Gimbutas. A numerical algorithm for the construction of efficient quadrature rules in two and higher dimensions. *Computers & mathematics with applications*, 59(2):663–676, 2010.
- [83] Jianguo Xin and Joseph E Flaherty. Viscous stabilization of discontinuous Galerkin solutions of hyperbolic conservation laws. *Applied Numerical Mathematics*, 56(3-4):444–458, 2006.
- [84] Jian Yu and Jan S Hesthaven. A study of several artificial viscosity models within the discontinuous Galerkin framework. *Communications in Computational Physics*, 27(5):1309–1343, 2020.
- [85] Jonas Zeifang and Andrea Beck. A data-driven high order sub-cell artificial viscosity for the discontinuous Galerkin spectral element method. *Journal of Computational Physics*, 441:110475, 2021.
- [86] Valentin Zingan, Jean-Luc Guermond, Jim Morel, and Bojan Popov. Implementation of the entropy viscosity method with the discontinuous Galerkin method. *Computer Methods in Applied Mechanics and Engineering*, 253:479–490, 2013.